Compositional engineering of metal halide perovskite for photo-sensing applications

M.Sc. Thesis

By
Kashish

Department of Physics
INDIAN INSTITUTE OF TECHNOLOGY INDORE
May,2024

Compositional engineering of metal halide perovskite for photo-sensing applications

A THESIS

Submitted in partial fulfillment of the

requirements for the award of the degree

of

Master of Science

by

Kashish

Department of Physics

INDIAN INSTITUTE OF TECHNOLOGY INDORE

May, 2024

INDIAN INSTITUTE OF TECHNOLOGY INDORE

CANDIDATE'S DECLARATION

I hereby certify that the work which is being presented in the thesis entitled **Compositional Engineering of hybrid halide perovskite for photo-sensing applications** in the partial fulfillment of the requirements for the award of the degree of **MASTER OF SCIENCE** and submitted in the **DEPARTMENT OF Physics, Indian Institute of Technology Indore**, is an authentic record of my own work carried out during the time period from 26 July 2023 to 31 May 2024 under the supervision of **Dr. Onkar Game, Professor, Indian Institute of Technology, Indore.**

The matter presented in this thesis has not been submitted by me for the award of any other degree of this or any other institute.

Kashish 22/5/24

Signature of the student with date
(Kashish)

This is to certify that the above statement made by the candidate is correct to the best of my/our knowledge.

OGame 22/5/24

Signature of the Supervisor of MSc thesis (with date)

(Dr. Onkar Game)

Kashish has successfully given his/her M.Sc. Oral Examination held on **16 May 2024**.

OGame 22/5/24

Signature of Supervisor of MSc thesis
Date:

Convener, DPGC
Date:

Dedicated to Almighty, my beloved parents and my family

ACKNOWLEDGEMENTS

I want to express my sincere gratitude to Dr. Onkar Game for his invaluable guidance, support, and encouragement throughout my project. Their expertise, insightful feedback, and unwavering commitment to excellence have been instrumental in completing this project.

I am highly thankful to Dr. Rupesh S. Devan who gave me access to complete my project in his lab. I am also thankful to each member of his lab who always supported me.

I want to acknowledge the Department of Physics, IIT Indore, for providing me with all the required research facilities.

I am grateful to my Ph.D. senior, Aayushi Miglani, who generously gave their time and expertise to contribute to this project. Their insights and perspectives were critical to the success of this project. I want to thank all the members of the AEMD group (Manjeet, Vaibhav, Nehansh) who helped me during this project.

I want to thank my parents and family members whose guidance and support always helped me throughout this journey.

I want to thank my friends, especially Naveen and Vishal, for their unwavering support, encouragement, and understanding throughout my project journey. Their love, motivation, and encouragement kept me going even during the toughest times.

Finally, I would like to acknowledge the infinite blessings of the Almighty, who has granted me the ability, knowledge, and opportunity to pursue my academic goals.

Thanks a lot, and once again, thank you for your support and guidance during this project.

ABSTRACT

Photodetectors convert light signals into electrical signals and are widely used in various applications like imaging, sensing and spectroscopy etc. Perovskites are widely used as an active layer in fabricating photodetectors because they show remarkable properties, such as low band gap, high light absorption coefficient, longer diffusion length, and higher carrier mobility. In addition to these properties, perovskite photodetectors have the advantage of simple and cost-effective fabrication and high performance, making them a better candidate for photodetection applications. Among various types of $CH_3NH_3PbI_3$ morphology (say single crystal, microwire etc.) $CH_3NH_3PbI_3$ microwires are particularly more useful for photodetection because of their lower defect density and highert mechanical flexibility. In this work, we successfully synthesized a lateral structure $CH_3NH_3PbI_3$ microwire photoconductor (ITO/ $CH_3NH_3PbI_3$/ITO) under ambient conditions and showed their various figure of merit. Further, to increase the response of this photodetector we synthesized polymer treated (PVP) photodetector which enhanced current by 1.44 times. Now, the stability of perovskite is the biggest issue of this time, so to enhance the stability of perovskite, we deposited a layer of a polymer PMMA, which not only enhanced its stability but also enhanced its photocurrent as well as various response parameters. This work opens the way toward improving stability and enhancing various response parameters of $MAPbI_3$ photodetector.

Contents

List of Figures:

List of Tables:

Chapter 1: Introduction

INTRODUCTION TO PHOTODETECTORS:

DEFINITION:

A photodetector is a device for detecting electromagnetic (EM) radiation *via* the conversion of an EM signal into a measurable electrical signal (voltage/current/power). The active material system used in a photodetector and its interaction with electromagnetic radiation dictates the region of the EM-spectrum that can be detected. Semiconductors are the most commonly used active material systems in photodetectors.

Unveiling Photoconductor-A type of Photodetectors:

Depending on the mechanism of conversion of EM-radiation to a measurable signal, photodetectors can be classified into 10-11 different types, including photoconductors, photodiodes, phototransistors, photomultiplier tubes, Charged Coupled Devices (CCDs), Complementary Metal-Oxide Semiconductor (CMOS), Pyroelectric, Thermopiles, etc.

In the section below we specify the Photoconductor type of photodetector that is relevant to the work of this thesis.

Photoconductor: A photoconductor is a type of photodetector that exhibits a change in its electrical conductivity when it is exposed to light.

This change occurs due to the reason that electrons in the valance band absorb energy from the incident photon and make a jump to the conduction band, generating an electron-hole pair. The presence of these electron-hole pairs increases the conductivity of the semiconductor. It means that more current can flow in light as compared to current in dark.

The duration for which this conductivity increases is known as persistence time. Since one photon absorbed can generate many photoelectrons so EQE higher than 100% is possible, according to the ratio between the charge recombination time (τ_r) and the charge transit time (τ_t) where transit times refers to the time take by electron or hole to reach at electrode from its point of generation), which is termed

photoconductive gain. Photoconductors have high gain because one type of charge carrier (say holes) can circulate through an external circuit many times before it recombines with its opposite carrier (say electrons) which meanwhile remain trapped in the photoconductor bulk as shown in Figure 1-1 [1].

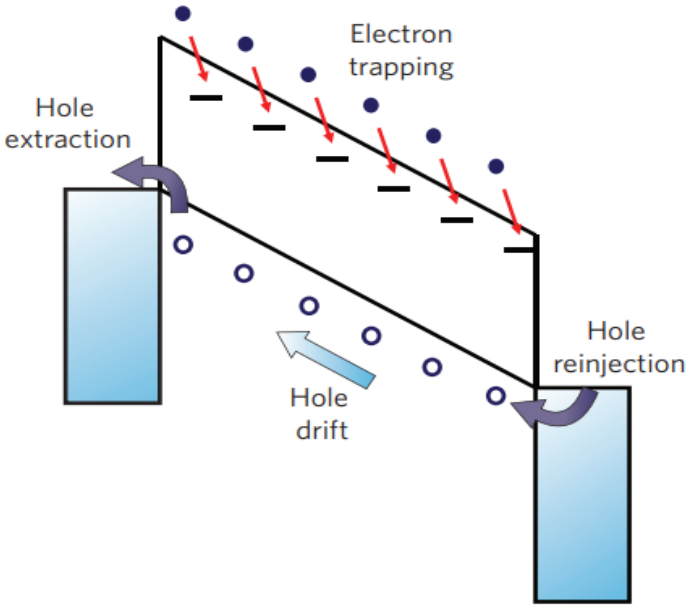

Figure 1- 1: In the photoconductor, a type of carrier gets trapped while the other responds to the applied field and keeps circulating as electrons are trapped in this figure. The electron capture from the conduction band into the trap state is represented by the red arrow. If transit time is shorter than the hole lifetime, then the longer lifetime of trapped electrons ensures the circulation of holes many times within an external circuit which is reason behind higher gain of photoconductors [1].

WORKING PRINCIPLE:

The photoconductors work on the principle that the conductivity of a material changes when it is exposed to light. This is known as the photoconductive effect. When a photoconductor is subjected to light, an electron-hole pair is generated, which can be separated by the application of external bias. Since absorption of a single photon could result in the generation of many conductible electrons, this type of photodetector shows higher photoconductive gain than photodiodes.

Under the application of applied bias, the electrodes can also inject charges, which can result in an EQE value of more than 100%.

TYPES OF PHOTOCONDUCTORS:

The fabrication method of photoconductors results in two distinct architectures: vertical and lateral.

Vertical structure Photoconductor:

The vertical structure photoconductor is developed as light-sensitive material between two electrodes. Usually, one of the electrodes is FTO/ITO so the light can enter the device while the back electrode is usually a metal. One can introduce an interlayer at one of the perovskite-metal or perovskite-electrode interfaces as a charge filtration layer as shown in Figure 1-2.

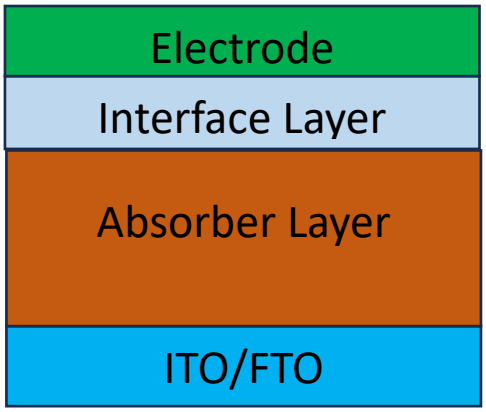

Figure 1- 2: The architectures represent the Vertical structure Photodetector.

Vertical structure photoconductors consist of multiple transport layers, so various trap states may exist in the interface of each transport layer, which may lead to many electron-hole recombination, lowering detection capabilities. Hence, vertical structure Photoconductor showes lower EQE and responsivity.

Lateral structure Photoconductor:

Light excites electron holes in the semiconducting layer (say Perovskite), which constitutes a current loop under an external electric field. Traps that capture electrons and these trapped electrons cannot contribute yo charge transportation but traps allow holes to pass within the device and external circuits

many times result in higher photoconductive gain. With the simplest structure, this photoconductor consists of two metal electrodes on either side of the semiconducting active layer, as shown in Figure 1-3.

`

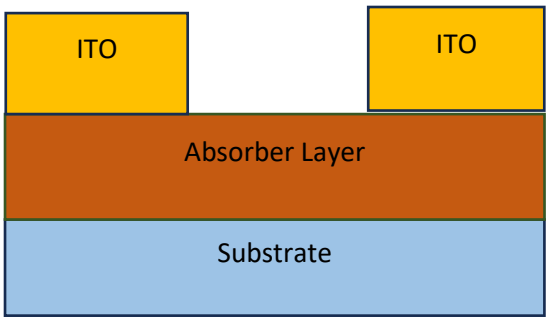

Figure 1- 3: The architecture represents the Lateral structure photoconductor.

As there is a significant distance between electrodes, photogenerated carriers take significant time to transfer from the generation site to the electrode, which results in higher response time and also shows the need of high driving voltage.

In the section below we will discuss the various figures of merits essential for determining a photoconductor's performance.

Photoconductor Performance Parameters:

Responsivity:

The responsivity of a photoconductor defines the photocurrent generated per unit power of incident light in the effective region of a photoconductor. It measures how effectively a photoconductor converts the incident light signal into an electrical signal. Responsivity is given as

$$\boldsymbol{R = \frac{I_{light} - I_{dark}}{P.A} = \frac{I_{ph}}{P.A}}$$

Where I_{dark} =Dark Current

I_{light}= light current generated by photodetector on illumination by light

$I_{light} - I_{dark}$=I_{ph}=Photocurrent

P=Power of incident light

A=Effective area of Photodetector

A higher responsivity indicates greater sensitivity, which means the photoconductor can detect weak signals effectively. An illustrative curve for Responsivity can be seen in Figure 1-4 [2] and a second example of this can be seen in Figure 1-5 [3] .Units of Responsivity:$Ampere/Watt$.

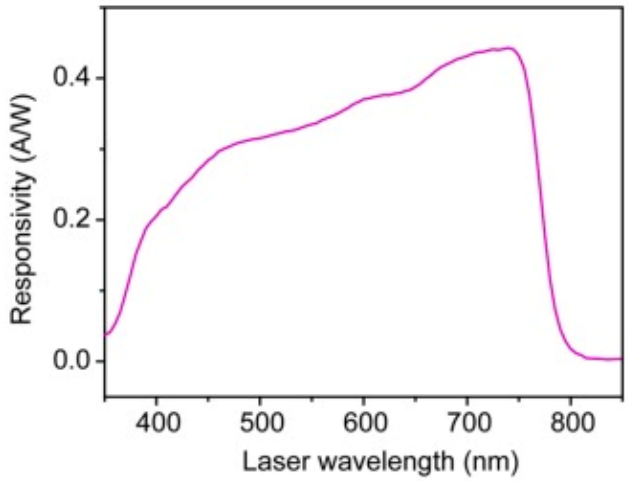

Figure 1- 4: A responsivity plot for lateral structure Methylammonium lead Iodide (ITO/$CH_3NH_3PbI_3$/ITO) photoconductor [2].

Detectivity:

Detectivity of any Photoconductor describes the ability of detector (or say photoconductor) material to detect weak light. It quantifies how effectively a photoconductor can differentiate between a signal of interest and inherent noise within the system. Detectivity is directly related to the signal-to-noise (SNR) ratio of photoconductors. The Responsivity and noise of the photodetector determine it. A higher detectivity leads to higher SNR ratio which is requirement for accurate measurement. Detectivity can be calculated as

$$D^* = \frac{\sqrt{A}R}{\sqrt{2eI_d}}$$

Where A= Effective area of Photodetector

R= Responsivity of Photodetector

I_d=Dark current

e= electronic charge

Detectivity sets the lower limit for detectable signal in a photoconductor system, providing a measure of its performance.

An illustrative curve for Detectivity can be seen in Figure 1-5 [3].

Units of Detectivity: $\frac{cm\sqrt{Hz}}{W} = Jones.$

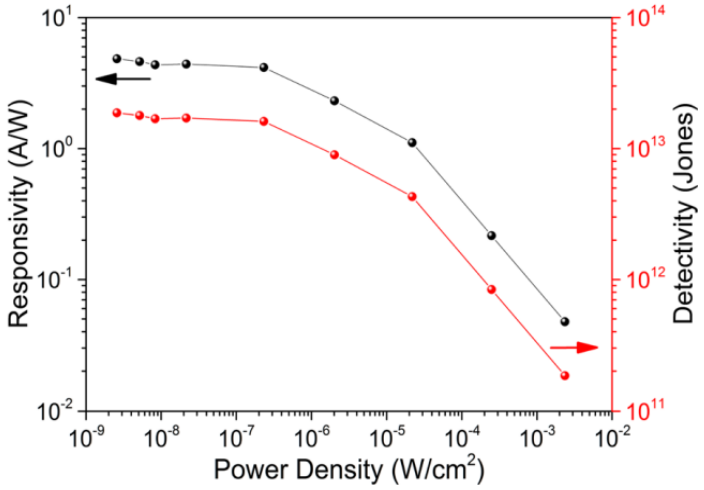

Figure 1- 5: A responsivity plot for Methylammonium lead Iodide nanowire structure photoconductor [3].

External Quantum Efficiency (EQE):

It is the ratio of output carriers to the number of incident photons per unit time. EQE is given as

$$EQE = \frac{I_{light}/e}{P/h\nu} = \frac{hR}{q\lambda}$$

Where ν =Frequency of applied signal.

λ= Wavelength of the applied signal.

q= charge of the carrier.

The curve for EQE can be seen in figure 1-6 [4].

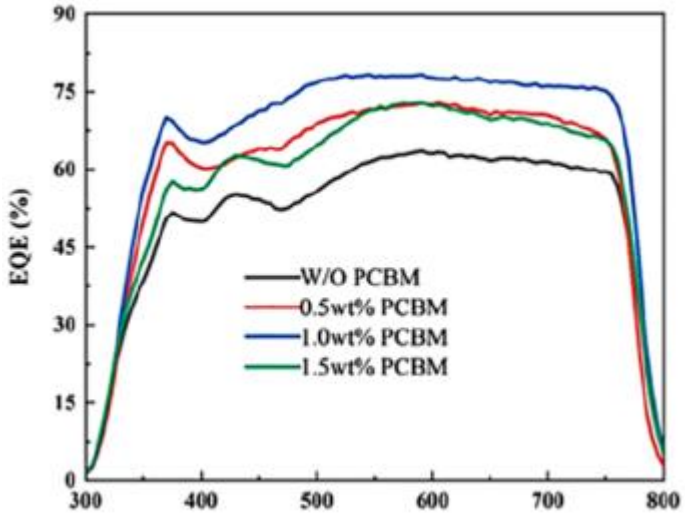

Figure 1- 6: EQE spectra for absorber layer with and without PCBM additive [4].

Also $0 < EQE < 1$ always. Higher EQE indicates greater sensitivity which further indicates a good Photoconductor.

Internal Quantum Efficiency (IQE):

It is defined as the ratio of photocurrent (in electrons per second) to photon fluence incident on the device (photons per second). It is related to responsivity via photon energy. IQE provides details into the effectiveness of a photodetector's internal processes, such as absorption, carrier generation, and carrier collection. IQE is given as

$$IQE = \frac{EQE}{n}$$

Where n= absorption coefficient of light

Higher IQE indicates greater sensitivity of photoconductors.

Linear Dynamic Range (LDR):

This indicates the linear association scale between the Photocurrent and light irradiance intensity. This defines the range of incident optical power levels over which the response of the photoconductor remains linear. Linear Dynamic Range (LDR) is given by the equation described below.

$$LDR = 20 \log \frac{I_{light}}{I_{dark}}$$

Figure 1-7 [5] shows the value of LDR measured from the current density versus optical power density plot.

A higher LDR values indicate that a photoconductor can perform better over a wide range of light intensities while maintaining a linear response.

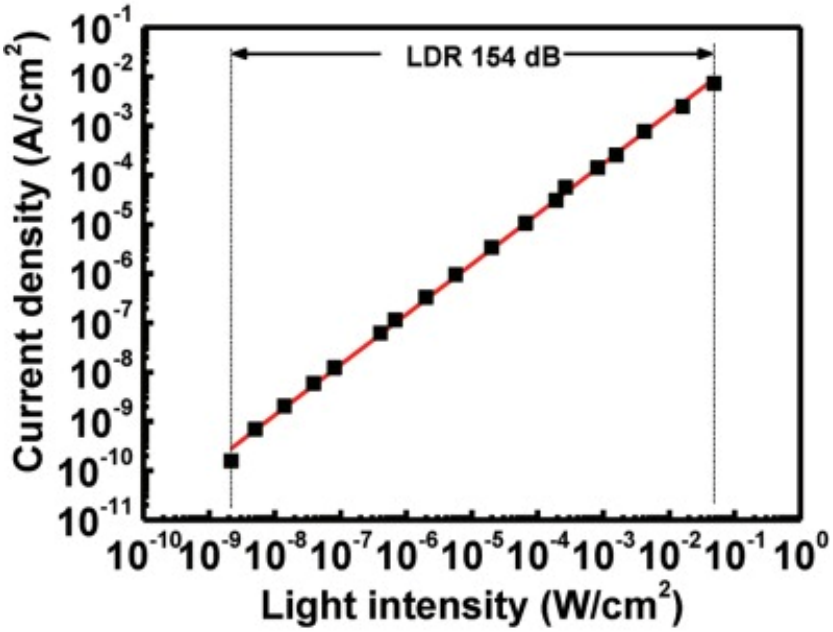

Figure 1- 7: The LDR for two photodetectors at zero bias [5].

Response Time:

The response time refers to the time taken by a photodetector to respond to an incident light signal. Due to variations in the intensity of incident light, Photocurrent there is a hysteresis in Photocurrent change. The rise time(τ_r) and fall time(τ_f) of photoconductor, give an estimation of time required for an photoconductor to respond to incident light signal.Where,

τ_r=rise time which means required to attain 10% to 90% of maximum current.

τ_f= fall time from 90% to 10% of maximum current.

An illustrative curve for the rise and fall time is shown in Figure 1-8 [2].

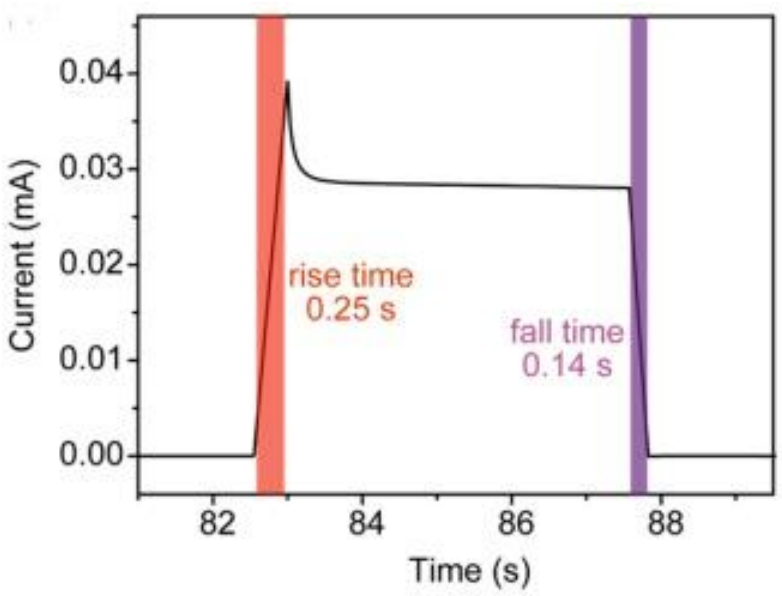

Figure 1- 8: The time-dependent Photo response of lateral structure Methylammonium Lead Iodide (Au/$MAPbI_3$/Au) Photoconductor at a +3V fixed bias [2].

A fast response time is crucial to accurately capture and process light signal changes.

The time it takes for detector output to change in response to a change in input light intensity is called apparent response time.

The approximate values of key parameters for specific types of photodetectors are presented in Table 1. These values serve as essential benchmarks, providing insights into the characteristics of Photodetector under consideration.

Table 1: Comparison between different Photodetector devices based on various response parameters.

Device Structure	EQE	R	D	Response Time	G	LDR	Driving Voltage	Photocurrent/ Dark Current
Photodiode	≤ 100%	Low	High	Short	Small	Large	Low	Low
Photoconductor	> 100%	High	Low	Long	Large	Narrow	High	High
Phototransistor	> 100%	High	Low	Long	Large	Narrow	High	High

Perovskites:

Introduction to Perovskites:

Metal halide perovskites have emerged as a class of semiconductors for high-performance solution-processed optoelectronics such as photovoltaics, Lasers, Light-Emitting diodes, etc. Perovskites are crystalline materials having a general formula ABX_3 where A and B are positively charged cations, and X represents a negatively charged anion. Ideally, perovskite crystallizes in a simple cubic crystal structure, which consists of a corner-sharing BX_6 octahedral network , as shown in Figure 1-9 [6].

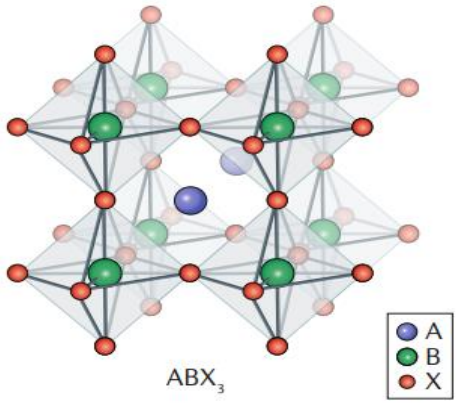

Figure 1- 9: 3D perovskite structure with general formula ABX_3 where A is a cation (say $CH_3NH_3^+$), B is metal (say Pb^{2+}), and X is an anion (say I^-). The arrangement of the crystal structure consists of a 3D network of corner-sharing PbI_6 octahedra where a 12-fold coordinated Pb surrounded by 8 octahedra occupies the middle position of the cube [6].

In the history of minerals, perovskites were first discovered by Gaustav Rose in 1839. The first perovskite found was $CaTiO_3$, named after Russian mineralogist L.A. Perovskiy. Later, many compounds like $BaTiO_3$, $PbTiO_3$, and $SrTiO_3$, etc., were found to show perovskite structure, and hence this class of materials was defined as Oxide perovskites with the general formula ABO_3. Generally, Oxide perovskite shows good ferroelectric, piezoelectric, and dielectric properties. However, they do not show good semiconducting properties except for a few compounds such as LiNbO3, PbTiO3, and BiFeO3, etc., which show some photovoltaic effect due to ferroelectric polarization.

Later, in 1893, a study was performed by Wells to replace the anion site of oxide perovskite with halide atoms, (Br, I, Cl). Then, in 1957, C. K. Moller, a Danish researcher, found that $CsPbCl_3$ and $CsPbBr_3$ crystallize in tetragonally distorted perovskite structures that makes a transition to a pure cubic phase at higher temperatures. This class of perovskite material was then said to be halide perovskite.

Further, in 1978, Dieter Weber replaced the A-site cation of halide perovskite with the organic compound Methylammonium ($CH_3NH_3^+$). He reported the first study on organic Lead halide perovskite $CH_3NH_3MX_3$ (where M=Pb, Sn and X= I, Cl, Br).

Then in 2009, For the first time, Prof. Miyasaka (Toin University of Yokohama, Japan) used perovskite (CH3NH3PbI3) as a light-harvesting layer in solar cells and reported the first perovskite solar cell showing an power conversion efficiency of 3.8%. Prior to this, no one had the idea that perovskite can be used to utilize solar energy because 2D perovskites are not suitable for light harvesting over a wide range of spectral range of sunlight.

Properties of Perovskites:

Various properties of perovskites make them better candidates for photovoltaic applications. A few of these properties are discussed below:

1. **Tunable bandgap:**
   Halide perovskites show tunable bandgap, which means that the bandgap of Perovskites can be adjusted by changing the chemical composition of Perovskite material. By selecting different cation and anion elements, bandgap of perovskite can be adjusted, and it can meet the necessity for a particular application.
2. **High absorption coefficient:**
   Due to the high absorption coefficient of Perovskite, they can absorb a large amount of incident light. This is beneficial for making thin Photodetectors with high sensitivity.
3. **Carrier mobility:**

Perovskite crystals can be grown with low defect densities, and they have low charge carrier trapping, which makes them show high carrier mobility, facilitating efficient charge transport of electrons and holes within the material.

4. **Long carrier lifetime:**
   These materials often exhibit long carrier lifetime, reducing the recombination rate and hence increasing the device's efficiency.
5. **Long Diffusion length:**
   Diffusion length is the average distance that a charge carrier travels before recombination. Hybrid halide perovskite has longer diffusion lengths, which allows it to travel more distances without recombination, which is advantageous for efficient charge collection at the electrodes of a photovoltaic device (say photoconductor).

In this work, we paid our attention to $CH_3NH_3PbI_3$ perovskite due to its various properties mentioned below:

The MAPI Perovskite:

The $CH_3NH_3PbI_3$ (MAPI) perovskite has attracted attention in perovskite due to its remarkable properties. This perovskite owns a direct bandgap of 1.5eV [7], High diffusion coefficient (1.59 to 2.41 cm^2s^{-1}) as well as High diffusion length of 14.0±5.1µm which leads to high carrier mobility 56.4-93.9 $cm^2V^{-1}s^{-1}$ [8]. Due to the perfect bandgap with band edge in the visible range and large absorption coefficient, the $MAPbI_3$ can be sensitive to wide spectra wavelengths from ultraviolet to visible light, which is beneficial for fabricating a broadband photodetector.

As we have discussed the properties of perovskites above and they are a good candidate for photovoltaic devices but for outdoor installation like Si PV panels, perovskite devices should be stable under real environmental conditions for a good period say approximately 20 years. Both extrinsic as well as intrinsic stability of perovskite is an issue. Environmental factors such as heat, light, humidity, and oxygen play an important role in the structural stability of perovskites. Different external environmental causes for perovskite degradation,

such as heat, light, and humidity, are critically important. Let's discuss them in detail:

Stability of Perovskites:

Structural/Intrinsic stability:

Goldschmidt tolerance factor (τ) gives an estimation of the structural stability of perovskite compounds and widely used to predict the formation of different crystal structures of ABX_3 The tolerance factor is given as $\tau = \frac{r_A + r_x}{\sqrt{2}(r_B + r_x)}$. Since ionic radii of organic cations (A) have some uncertainties in their measurements so there must lie some uncertainty in tolerance factors. Figure 1-10 [9] shows the calculated tolerance factors of $APbI_3$ systems where A = Na, K, NH_4, Rb, Cs, MA, FA, EA (ethylamine), and EDA (ethylenediamine). When the tolerance factor spans within the range $0.8 < \tau < 1$, cubic perovskite structures or distorted structures like tilted octahedra are favored. Between $0.9 < \tau < 1$ a favor for cubic structure emerges whereas within range $\tau < 0.8$ and $\tau > 1$ inhibit the formation of perovskite structure leading to non-perovskite phase formation.

External/Environmental stability:

Ensuring the stability of the perovskite to external conditions like moisture, oxygen (air), heat, light, external bias, etc., is a crucial factor after obtaining the proper stable structural phase of perovskites. The moisture sensitivity of perovskite is a serious concern for its long-term stability. It's understood that water molecules easily form hydrogen bonds with perovskite to make them hydrated compounds that induce localized alteration in their properties.

The equations below show the mechanism for the poor stability of $MAPbI_3$ perovskite in external conditions. It shows that $MAPbI_3$ reacts with water and gets converted into PbI_2.

$$4CH_3NH_3PbI_3 + 4H_2O \leftrightarrow 4[CH_3NH_3PbI_3.H_2O] \leftrightarrow (CH_3NH_3)_4PbI_6.2H_2O + 3PbI_2 + 2H_2O$$

$$(CH_3NH_3)_4PbI_6.2H_2O \rightarrow 4CH_3NH_3I + PbI_2 + 2H_2O$$

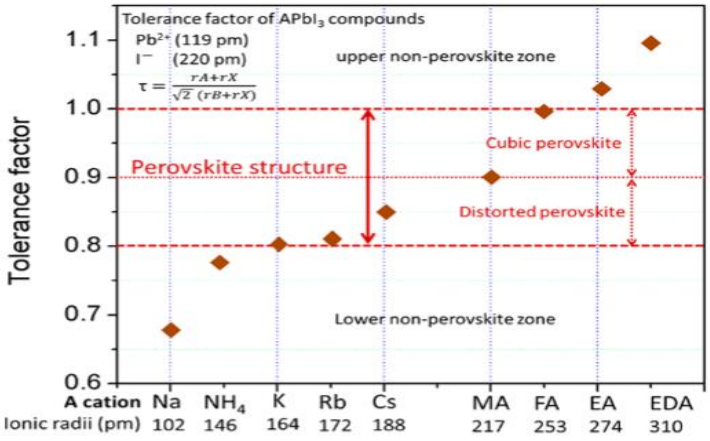

Figure 1- 10: Calculated tolerance factors (τ) for different cations (A) in the $APbI_3$ perovskite system [9] .

Therefore, a proper encapsulation is needed to prevent perovskite devices from moisture. Nonetheless, many efforts are made to protect perovskite from external moisture by introducing moisture resistance material in perovskite devices.With a minimal cost, it is possible to prevent perovskite from external humidity.

<u>Polymer passivation</u>:

Defect states/traps have a significant role in the charge transportation through of perovskite photodetectors. Within a semiconductor, a defect/ trap state denotes any irregularity that generates localized states positioned around the site of imperfection and energetically situated within the band gap of the semiconductor. These traps exhibit different depths, termed shallow if they are near the band edge or deep if they are located far away from the band edges within the band gap. For instance, abundant traps may also exist at grain boundaries where swinging bonds form deep defect states and affect charge transportation in perovskites. These defects lead to non-radiative loss leading to low device performance. Further, it is shown experimentally that many trap defect densities in polycrystalline perovskite film are on the order of 10^{16}- 10^{17} cm^{-3} [10]. Further, as we discussed perovskite is very sensitive to light, moisture, and humidity. It is also shown experimentally that defects at grain boundaries and interfaces of polycrystalline perovskites provide a path to hydration of perovskites to form $(CH_3NH_3)_4PbI_6.2H_2O$ [11]. It is also verified that GB defects lead to irreversible

moisture-induced perovskite degradation [12]. Polymer passivation is the right approach to resolve these issues. Polymer encapsulation acts as a barrier for moisture, humidity, and light to reach the perovskite directly. Long-range polymers passivate GB defects occurred due to swinging bonds by making a stable interface with perovskite material.

Chapter 2: Experimental Work-Stage 1

Experimental procedure:

Formation of microwires:

All raw materials (MAI, PbI_2, and DMF) were purchased from TCI chemicals. The Methylammonium lead iodide precursor solution was prepared by dissolving an equimolar amount of MAI (Methylammonium iodide) and PbI_2(Lead iodide) in DMF (N, N-Dimethylformamide). The solution was kept overnight for stirring. The precursor was further filtered with $0.45\mu m$ PTFE filter. ITO substrates (size 1.5cm ×2.5 cm) were washed with soap solution, DI water, Acetone, and IPA (isopropanol) with sonication for 15 minutes each and then treated with UV ozone for 20 minutes. Following this, 60 µL of the precursor was spin-coated at 4000 rpm with 2000 rpm/sec acceleration. After this, all the substrates were annealed at 100^0C for 10 minutes.

Characterization:

The prepared $CH_3NH_3PbI_3$ microwires were characterized by SEM and XRD. Various monochromatic light sources performed optoelectronic characterization, and Keithley 2450 SMU was used. All the optoelectronic measurements were performed in a completely dark box.

Results and Discussions stage 1:

The $MAPbI_3$ has a perovskite structure, and the XRD of this is shown in figure 2-1 below.

The XRD of $MAPbI_3$ microwires has two main peaks at 14.08^0 and 28.39^0, which can be indexed to (110) and (220) planes of perovskite structure like results reported by others [3]. The $MAPbI_3$ material crystallizes in the tetragonal phase (a=9.2825Å and c= 11.90Å) and this also matches with existing literature reported by others. The peaks denoted by # represent the peak due to the ITO substrate. As seen from XRD data, the signals occurring at (110) and (220) planes are highly intense, which states that growth is along the (110) family.

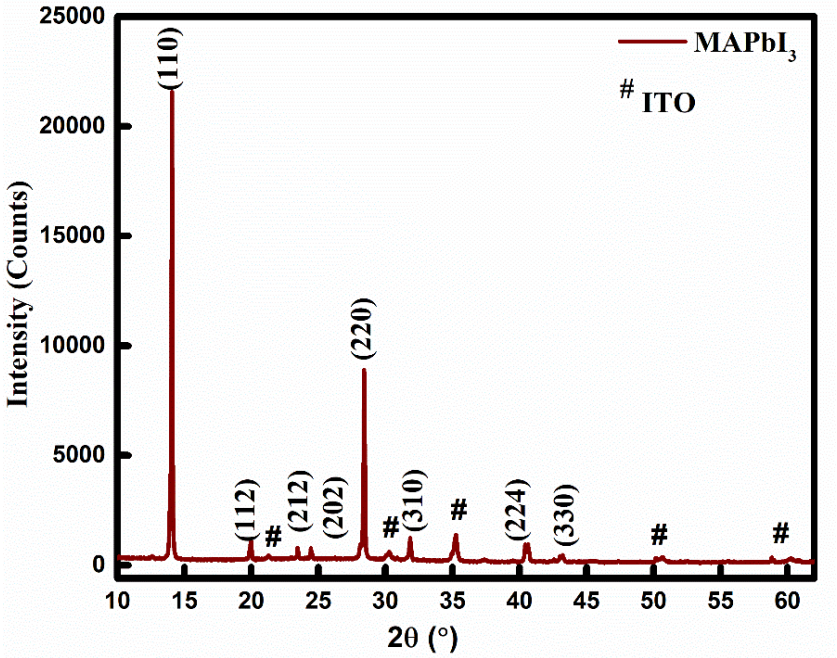

Figure 2- 1: The plot shows the XRD pattern for $MAPbI_3$ microwires.

Further, Using Debye-Scherrer equation we can estimate the crystallite size and this equation is given as:

$$D = \frac{k\lambda}{\beta \cos\theta}$$

Where k is Scherrer constant and for tetragonal phase k=0.89

β is FWHM of peak in radians.

λ is Wavelength of incident X-rays which is 1.5426Å.

θ is Bragg's angle.

From the obtained XRD pattern for MAPbI3 microwires and computing FWHM from the most intense signals, we get the crystallite size given in the table below.

Further, using Bragg's law which states

$$2d \sin\theta = n\lambda, \text{ where } d = \frac{1}{\sqrt{\frac{h^2}{a^2}+\frac{k^2}{b^2}+\frac{l^2}{c^2}}}$$

2θ(Degrees)	FWHM (Radians)	Crystallite size D (nm)
14.08	0.00183	75.5296
28.42	0.00238	59.4537
		$D_{avg.}$=67.492

we calculate lattice parameters, and which are shown in table below and in Bragg's law d is interplanar spacing, θ is Bragg's angle and λ is wavelength of X-rays.

S.No.	(hkl)	$2\theta(degrees$	Interplanar spacing (Å)	Lattice parameter (a=b) (Å)	Lattice Parameter (c) (Å)
1	110	14.07495	6.2626	8.86	
2	220	28.41831	3.1313	8.86	
3	112	19.99	4.4430		12.599
4	212	23.44	3.3491		11.36
5	202	12.22	3.6555		11.74
6	310	28.4	3.1482	9.95	
7	224	31.84	2.8150		
8	330	40.53	2.2292	9.46	

Table 3: Estimation for lattice parameters of $MAPbI_3$ using XRD data.

Further, on computing the average of the obtained result, we get a=b= 9.2825Å and c= 11.90Å.

SEM image showing $MAPbI_3$ sample coated on ITO is shown in Figure 2-2 below. We can see the bundles of microwire images from SEM images. Now, these bundles of wires are connected horizontally to each other, which allows effective charge transport along this direction and makes this architecture beneficial for lateral photoconductors.

(a)

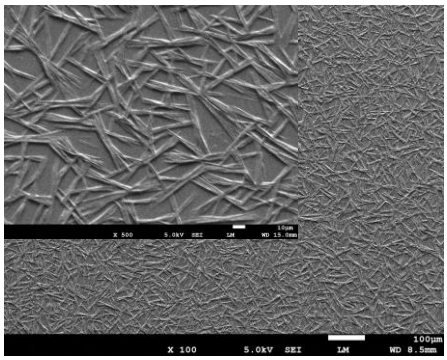

(b)

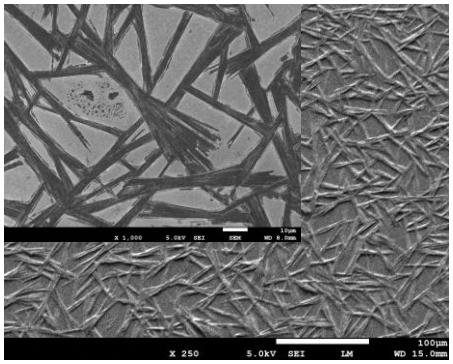

(c)

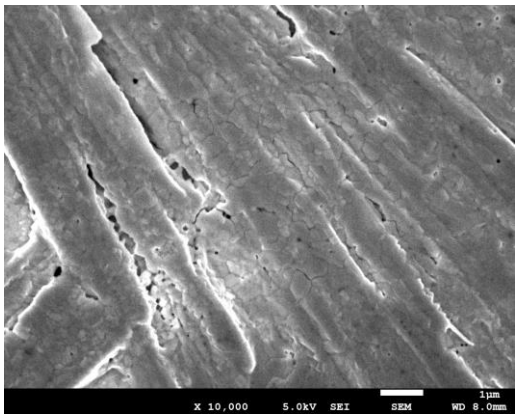

Figure 2- 2: The SEM image of $MAPbI_3$ microwires.

Using ImageJ software, we analyzed our FESEM images and calculated the mean length of MAPI microwires to be 35.93 μm as shown in Figure 2-3.

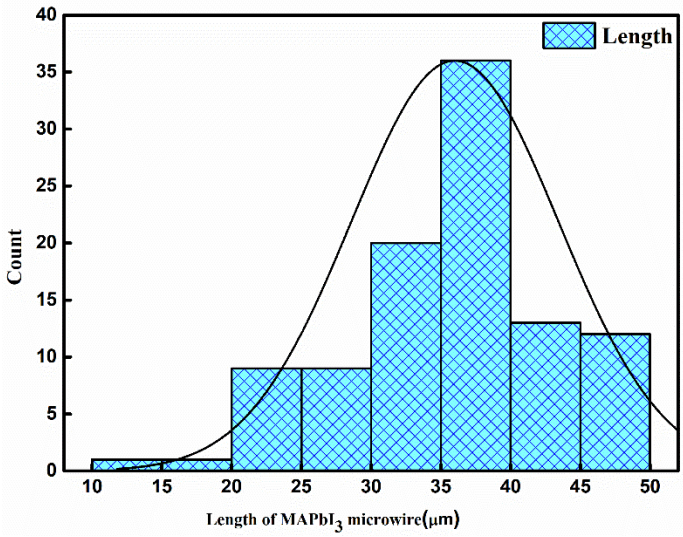

Figure 2- 3: To find out the mean length of the microwires.

Further in this work, we measured various response parameters for $MAPbI_3$ photoconductor, but prior to this, let's have a look at the band diagram of MAPbI3 as shown in Figure 2-4. The band gap of $MAPbI_3$ is 1.5eV. An electron in the lower energy level (valance band) receives energy and jumps to the upper energy level, creating an electron-hole pair. Further electrons by means of applied bias are attracted towards the ITO side, and in a similar fashion, holes in lower levels also move towards the ITO side by generating current in the device, which results in the increase of the conductivity of the photoconductor.

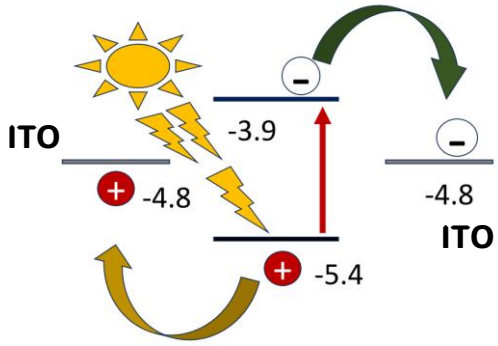

Figure 2- 4: Energy level diagram of materials ($MAPbI_3$ and ITO) used in our work.

Under white light illumination at 4V bias, we found the photocurrent of this photoconductor to be 1.47μA and three orders of magnitude change from dark current to light current, as shown in Figure 2-5 below.

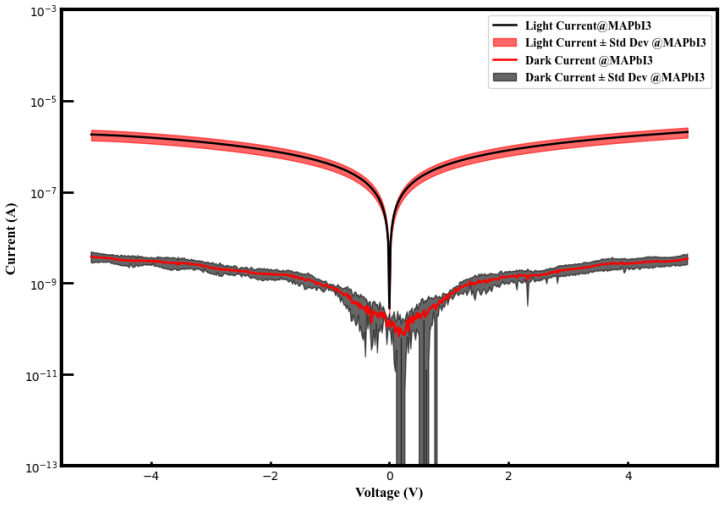

Figure 2- 5: Photo-response of $MAPbI_3$ photoconductor for -5 to 5V voltage scan under white light illumination.

Further, to check the wavelength-dependent response of our device, we measured its IV characteristics at various wavelengths from IR to near UV range, which can be seen in Figure 2-6 below.

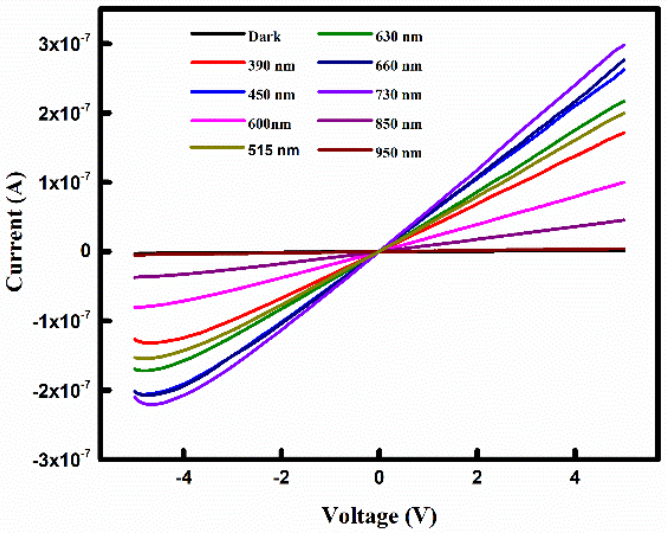

Figure 2- 6: IV curves of $MAPbI_3$ microwire structure under dark and various monochromatic lights.

From the plot, it can be seen that the device exhibited dark current in nano-ampere and light current in micro-ampere. Also, Figure 2-7 (IV characteristics on a logarithmic scale), as figures show that the device exhibits almost 2 to 3-order magnitude changes from dark to light current except for 850nm and 950nm because these wavelengths lie lower than the band-edge of $MAPbI_3$.

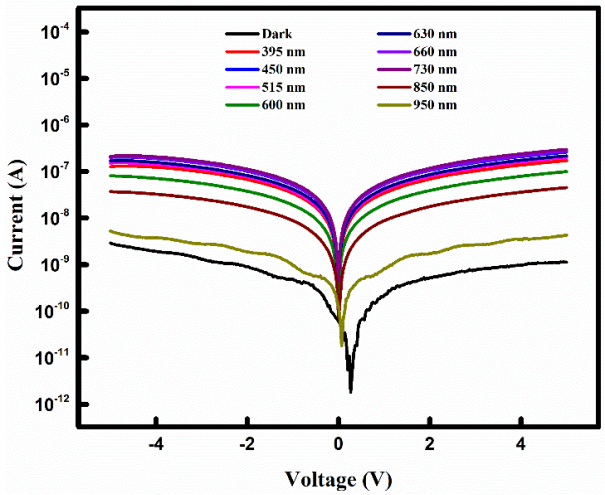

Figure 2- 7: Logarithmic scale IV curves of $MAPbI_3$ microwire structure under dark and various monochromatic lights.

Then, we calculated the responsivity and detectivity of our device at various wavelengths, which can be seen in Figures 2-8 and 2-9 below. This responsivity matched to some extent with already reported literature [13].

From the literature that has already been reported, we find that the MAPbI3 photodetector is more responsive at a wavelength near 550nm than others [14], which can also be seen in Figures 5-8. So, we tried to check the response of our device at 515nm and calculated its various response parameters which are discussed below.

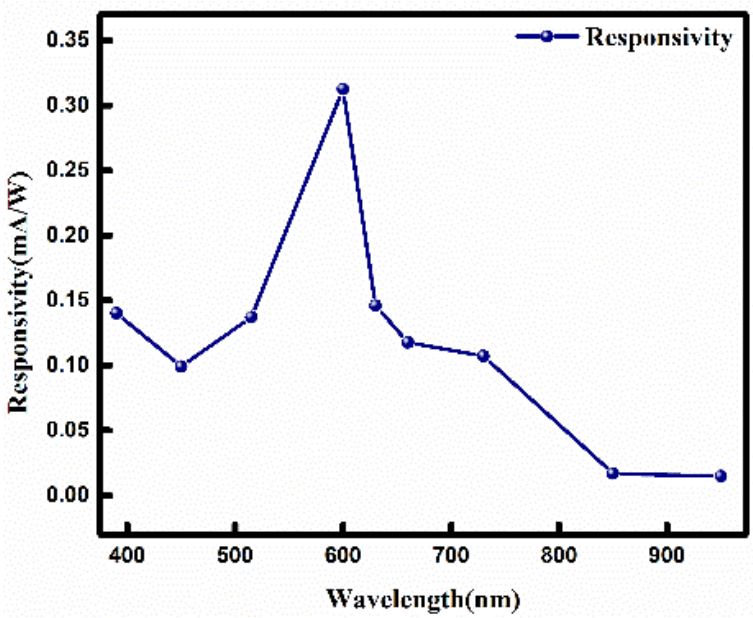

Figure 2- 8: The curve for Responsivity at various wavelengths ranging from 390 nm to 950 nm at a fixed bias of 4V.

Under monochromatic 515nm light illumination, our device exhibited a light-to-dark ratio of 1330.77, as shown in Figure 2-10.

Further normalized Current versus time was plotted (figure 2-11) to calculate rise and fall time from which rise time of 3.152 sec and fall time of 0.217 sec were calculated. The reason for a higher rise time than fall time is that in lateral structure photoconductors, lateral charge transport involves longer pathways, leading to a slower rise time compared to fall time when charges are collected.

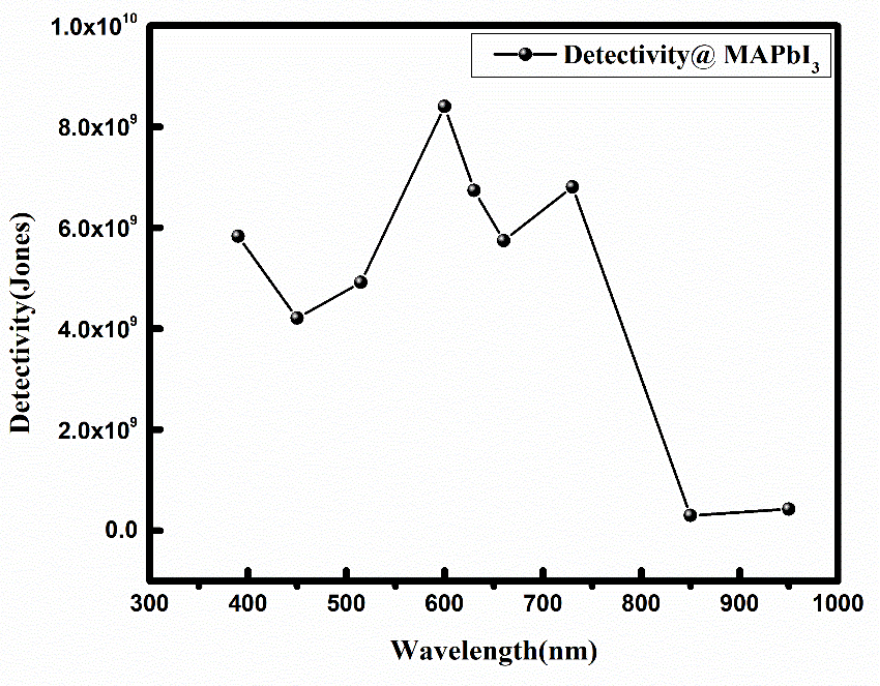

Figure 2- 9: The curve for Detectivity at various wavelengths ranging from 390 nm to 950 nm at a fixed bias of 4V.

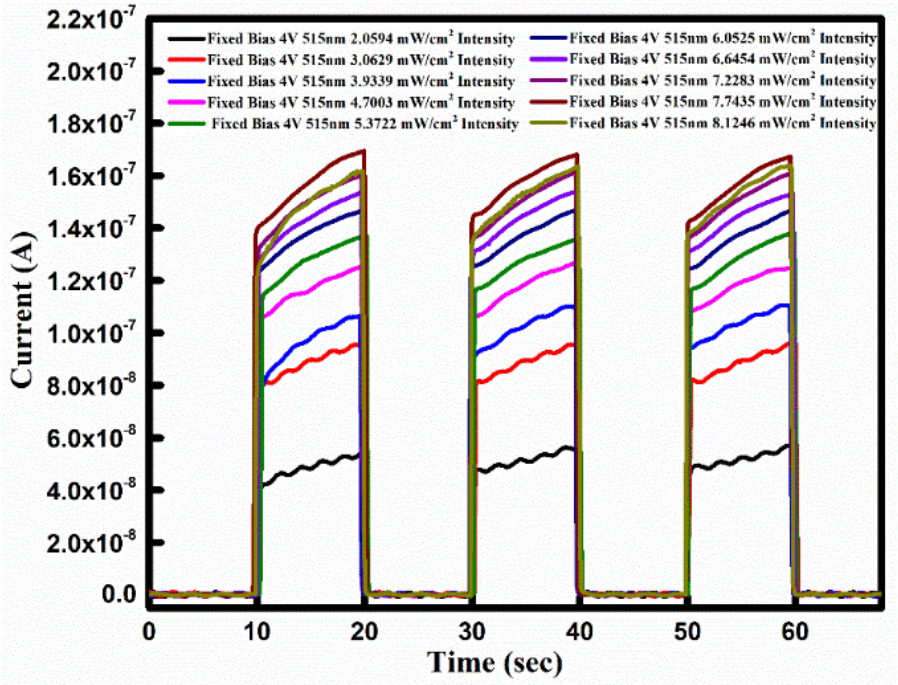

Figure 2- 10: Light-dark current curves of $MAPbI_3$ under 515nm monochromatic light illumination at a fixed bias of 4V.

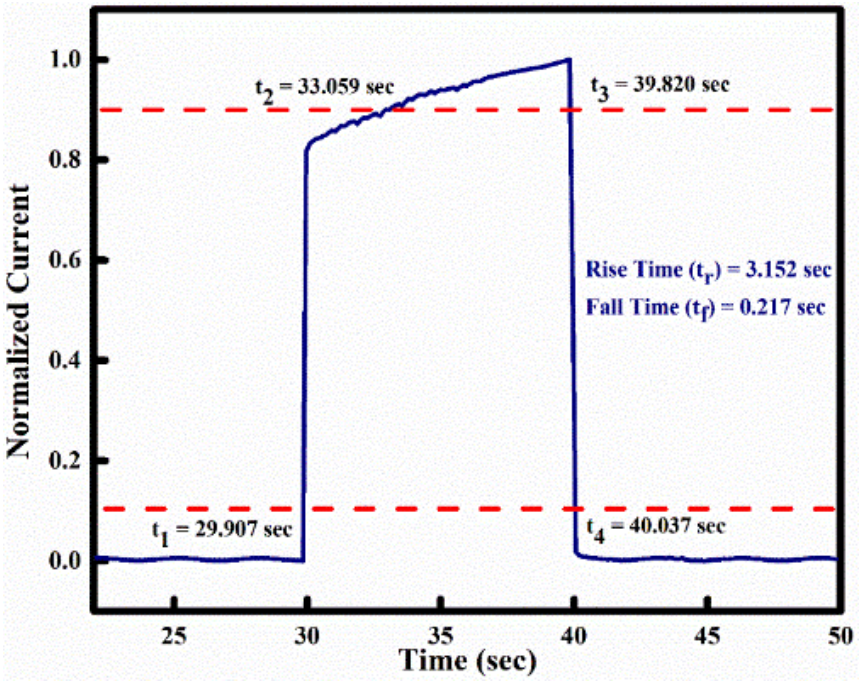

Figure 2- 11: The normalized photocurrent over a varied duration of time at incident light of 515nm with an 8.1246 mW/cm^2 intensity for calculation of rise and fall time of $MAPbI_3$ devices.

Further, the curves show the responsivity and detectivity of the device at various wavelengths Figure 2-12. The device showed 0.18 mA/W responsivity and 1.12×10^{10} jones detectivity at 3.93mW/cm^2 intensity of incident 515nm light.

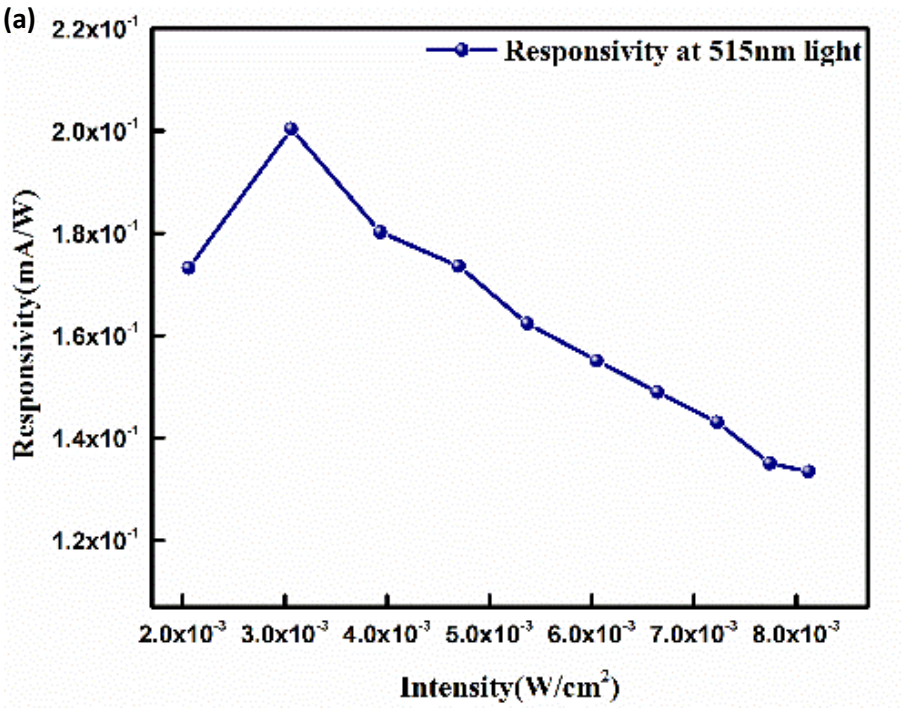

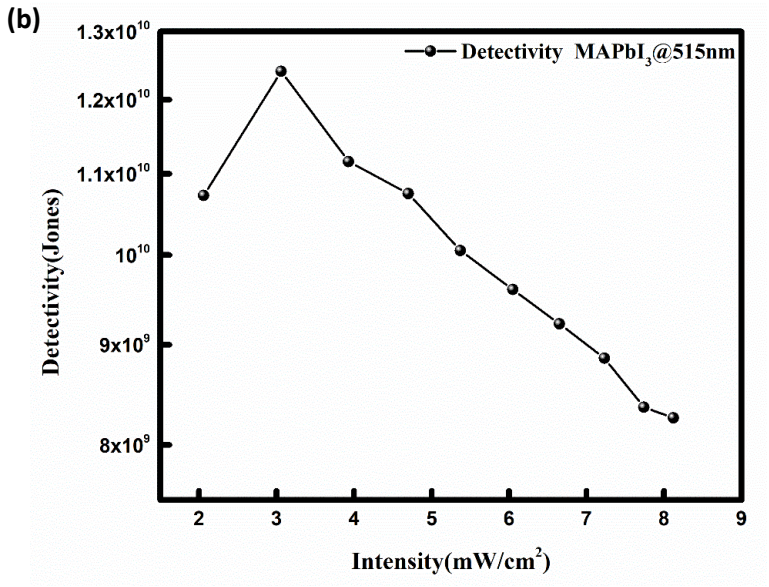

Figure 2- 12: (a) The plot for Responsivity variation with optical power density under 515nm monochromatic light illumination. **(b)** The plot for Detectivity variation with optical power density under 515nm monochromatic light illumination.

The LDR is an important figure of merit for photoconductors, which tells the range for which the response of the photoconductor is in a linear relationship with incident optical power density or Intensity. As shown below, our device is getting an LDR of 125 dB. The higher LDR ensures precision and accuracy in converting incident light to electrical signals, as well as a high signal-to-noise ratio, allowing the accurate detection of weak signals.

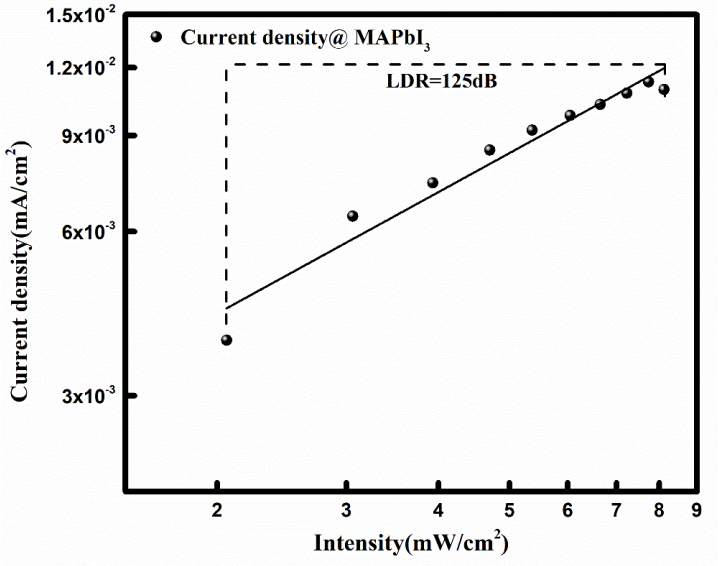

Figure 2- 13: The plot for Current versus Intensity for $MAPbI_3$ using 515nm wavelength light at fixed 4V bias for calculation of LDR.

Further, as we discussed above, EQE (external quantum efficiency) specifies the number of output carriers generated to the number of incident photons per unit time. So, figure 2-14 shows the EQE of this device at various wavelengths. We measured 38.86% of the maximum EQE at 600nm.

Further, we calculated the EQE at 515nm with variation in intensity, which can be seen in Figure 2-15 below.

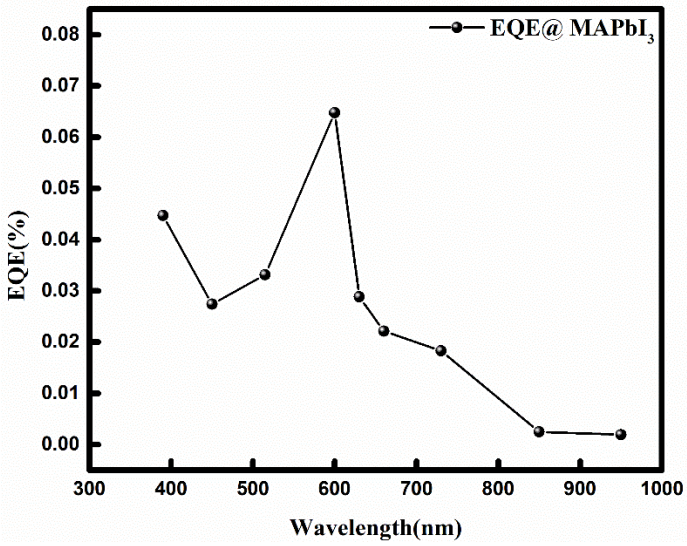

Figure 2- 14: The plot for Wavelength versus EQE for $MAPbI_3$.

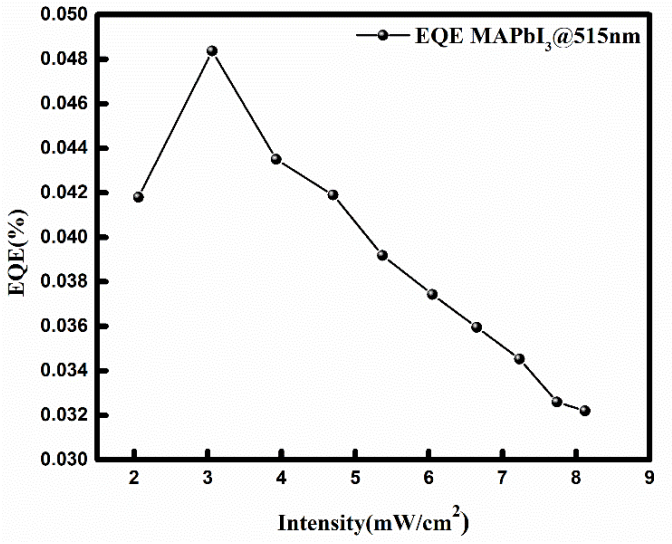

Figure 2- 15: The plot for EQE versus Intensity for $MAPbI_3$ using 515nm wavelength light at fixed 4V bias.

Chapter 3: Experimental Work-stage-2

Experimental procedure:

Formation of polymer-treated devices:

All raw materials (MAI, PbI_2, DMF, PVP, PMMA, and toluene) were purchased from TCI chemicals. The Methylammonium lead iodide precursor solution was prepared by dissolving an equimolar amount of MAI (Methylammonium iodide) and PbI_2(Lead iodide) in DMF (N, N-Dimethylformamide). The PVP in ratio MAI: PVP (1000:1) was also dissolved in this solution. The solution was kept overnight to stir at room temperature. The PMMA with 20mg/ml in toluene was prepared and kept overnight, stirring at room temperature. The $MAPbI_3$ precursor was further filtered with 0.45μm PTFE filter. ITO substrates (size 1.5cm ×2.5 cm) were washed with soap solution, DI water, Acetone, and IPA (isopropanol) with sonication for 15 minutes each, and then they were treated with UV ozone for 20 minutes. Following this, 60 µL of PVP mixed $MAPbI_3$ precursor was spin-coated at 4000 rpm with 2000 rpm/sec acceleration. After this, all the substrates were annealed at 100^0C for 10 minutes. Following this, these substrates were dynamically treated with PMMA at 2000rpm with 2000rpm/sec acceleration, and PMMA was allowed to get distributed on the substrate at this speed for 40 seconds. Then these substrates were annealed at 100^0C for 1-2 minutes.

Results and Discussions Stage 2:

As we discussed above, different trap states lead to non-radiative losses, which reduces the performance of the device. Also, abundant traps may also exist at grain boundaries where swinging bonds form deep defect states and affect charge transportation in perovskites. So, in the leading section, we will first discuss the importance of defect passivation.

Importance of defect passivation in perovskites:

The photoconductor works on the principle that a change in electrical conductivity of active layer material or semiconductor occurs when it is subject

to light, which has energy greater than the band-edge of active material (perovskite in this work). The perovskite layer absorbs the incident photon, which results in the excitation of an electron from the valance band to the conduction band, creating an electron-hole pair as shown in Figure 3-1 by process 1 [14].

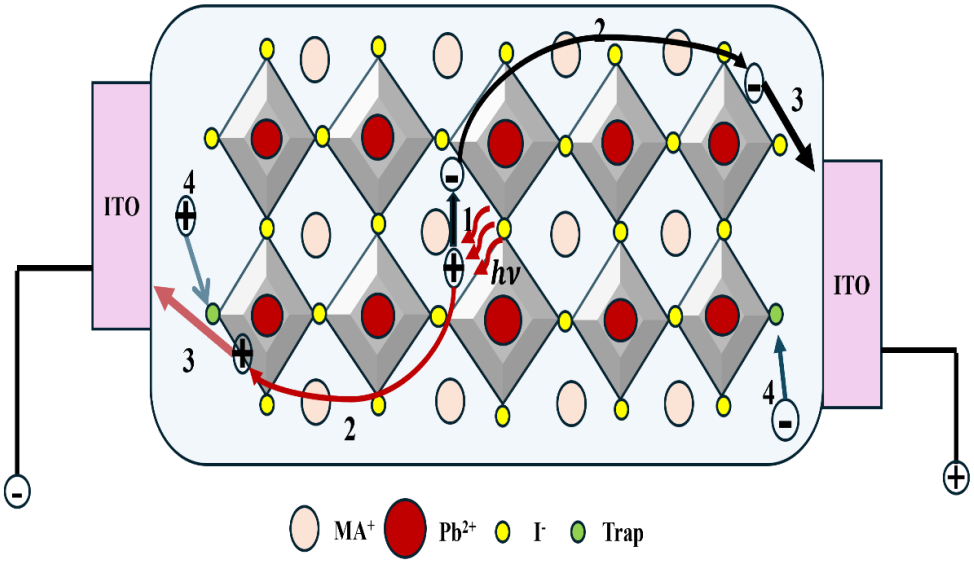

Figure 3-1: Schematic working of $MAPbI_3$ photoconductor.1) Generation of electro-hole pair by absorbing some energy 2) Diffusion of charge carries through perovskite material under the application of applied bias 3) Extraction of charge carriers at electrodes 4) Recombination of charges carriers due to existence of trap states[14].

These electron-hole pairs can be separated into free charges by providing lower exciton binding energy close to thermal energy at room temperature ($K_BT \approx$ 26meV) which enables an efficient charge separation by thermal dissociation. These free carriers diffuse through perovskite material, as shown by process 2 in Figure 3-1 above, and are further transported to electrodes, as shown in process 3. However, the effective collection of charge carries depends on carrier lifetime. Practically, before extraction of free charges, they may undergo non-radiative recombination processes, which lead to lower efficiency of the photoconductor. The defects that impact the device performance mainly are 0D defects (impurities and Vacancy etc.) and 2D defects (grain boundaries and surface defects). Grain boundaries (2D defects) in perovskite cause sudden changes in crystal orientation, producing many localized surface states that act as trap sites. Further,

Beard and co-workers have proved that in $MAPbI_3$ perovskite, surface recombination is more important than recombination within the crystal [15], [16].

So, from the existing literature, we concluded that PVP provides an effective method for passivating perovskite layers whose defect density is reduced, suppressing recombination. Due to this, PVP passivation helps in the growth of perovskite films with lower grain boundary density, giving low non-radiative recombination centers [17]. So, to passivate our device, we tried coating PVP along with $MAPbI_3$.The results are discussed below:

Under white light illumination at 4V bias, we found the photocurrent of this photoconductor to be $2.12\mu A$ and three to four orders of magnitude change from dark current to light current as shown in Figure 3-2 below:

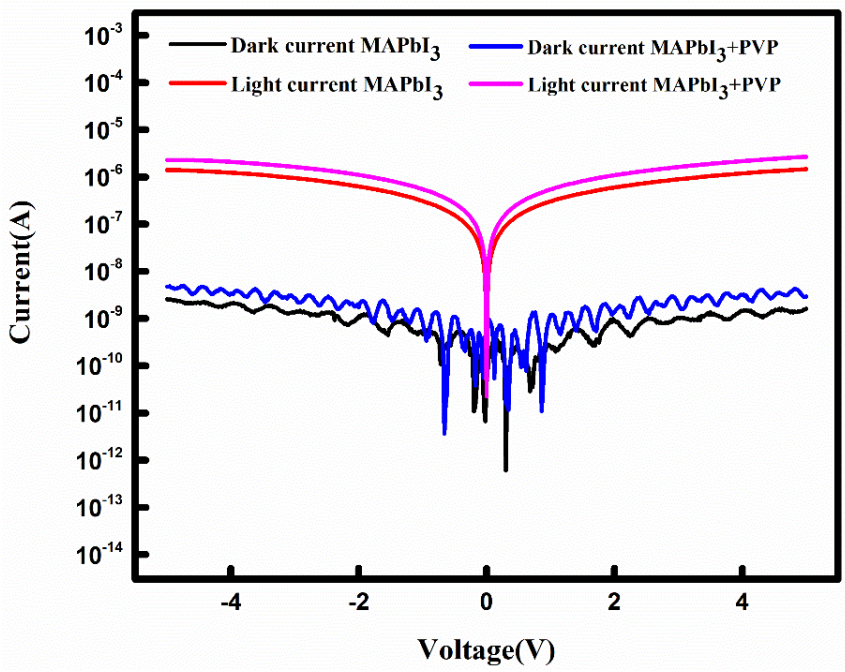

Figure 3- 2: Photo-response of $MAPbI_3$+PVP photoconductor for -5 to 5V voltage scan under white light illumination.

Further normalized Current versus time was plotted in Figure 3-3 to calculate rise and fall time, from which a rise time of 0.468 sec and fall time of 0.146 sec was calculated. The reason for a higher rise time than fall time is that in lateral structure photoconductors, lateral charge transport involves longer pathways, leading to a slower rise time compared to fall time when charges are collected.

Further, we characterized this device as an IV measurement as days progress till their degradation. The data for the same can be seen in Figure 3-4. Although this device exhibited a higher photocurrent as well as improved rise and fall time than pristine $MAPbI_3$, the stability issue was still the same as earlier. As we can see from the plot, both types of devices could last only six days and started degrading on the fourth day by showing a one-order magnitude change in photocurrent when stored under ambient conditions.

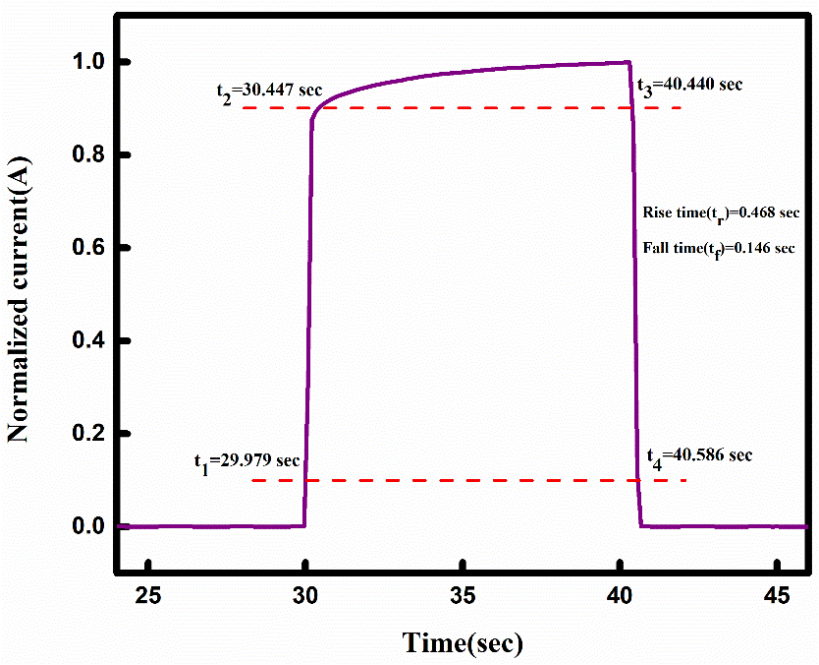

Figure 3- 3: The normalized photocurrent over a varied duration of time at incident light of 515nm with an 8.1246 mW/cm^2 intensity for calculation of rise and fall time of PVP-treated $MAPbI_3$ devices

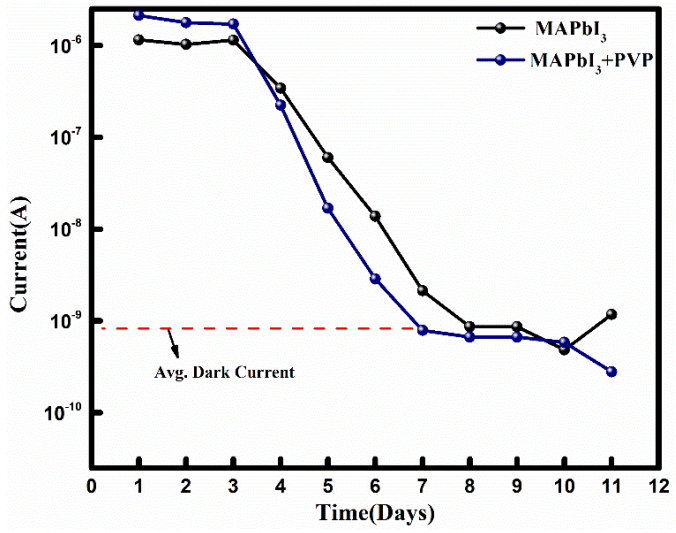

Figure 3- 4: Number of days versus photocurrent exhibited by polymer passivated (PVP) and pristine $MAPbI_3$ photoconductor.

Further, to enhance the stability of this device we post-treated this pristine $MAPbI_3$ with PMMA and characterized it for IV characterization shown in Figure 3-5 below:

Under white light illumination at 4V bias, we found the photocurrent of this photoconductor (ITO/ $MAPbI_3$+PVP+PMMA/ITO) to be 1.65 μA and approximately three to four orders of magnitude change from dark current to light current, as shown in Figure 3-5 above. Treatment of PMMA enhanced the photocurrent, so to check the wavelength-dependent response of our device, we measured its IV characteristics at various wavelengths from IR to near UV range, which can be seen in Figure 3-6 below. From Figure 3-6, it can be seen that the device exhibited dark current in nano-ampere and light current in micro-ampere.

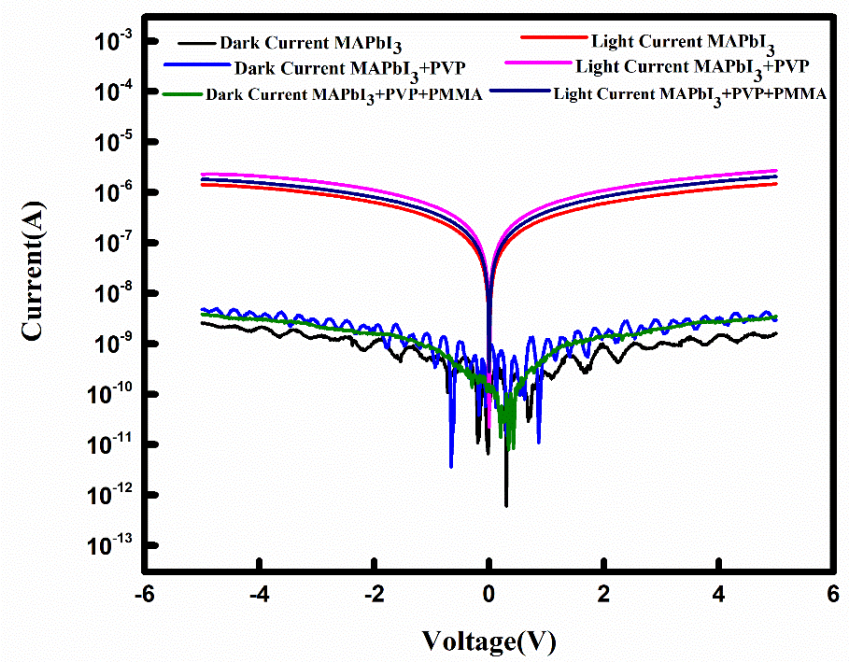

Figure 3- 5: Photo-response of $MAPbI_3$+PVP+PMMA photoconductor for -5 to 5V voltage scan under white light illumination.

Also, from Figure 3-7 (IV characteristics on a logarithmic scale) shows that the device exhibits almost 2 to 3-order magnitude changes from dark to light current except for 850nm and 950nm because these wavelengths lie lower than the band-edge of $MAPbI_3$.

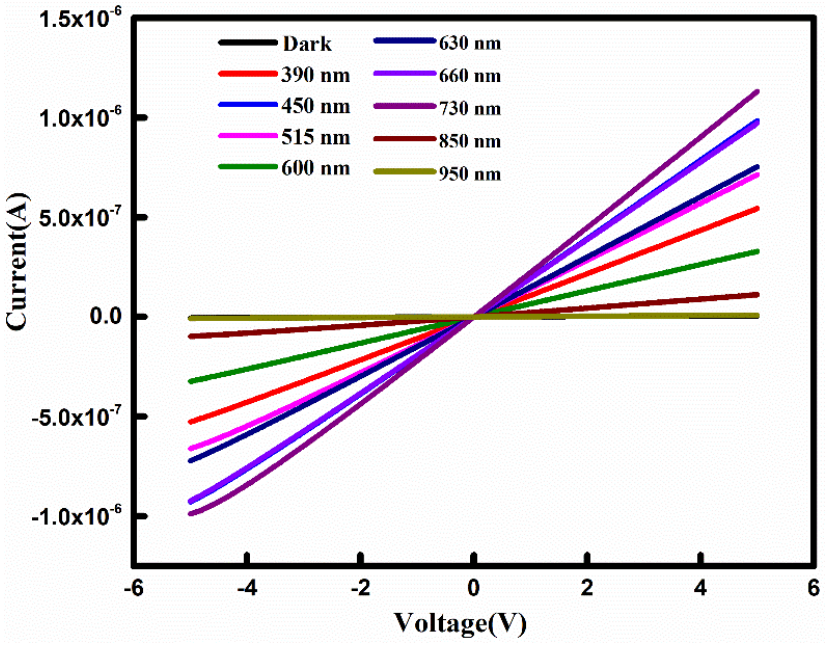

Figure 3- 6: IV curves of $MAPbI_3$+PVP+PMMA photoconductor under dark and various monochromatic lights.

Then, further, to compare our device with a pristine $MAPbI_3$ photoconductor, we calculated responsivity and detectivity at various wavelengths as shown below.

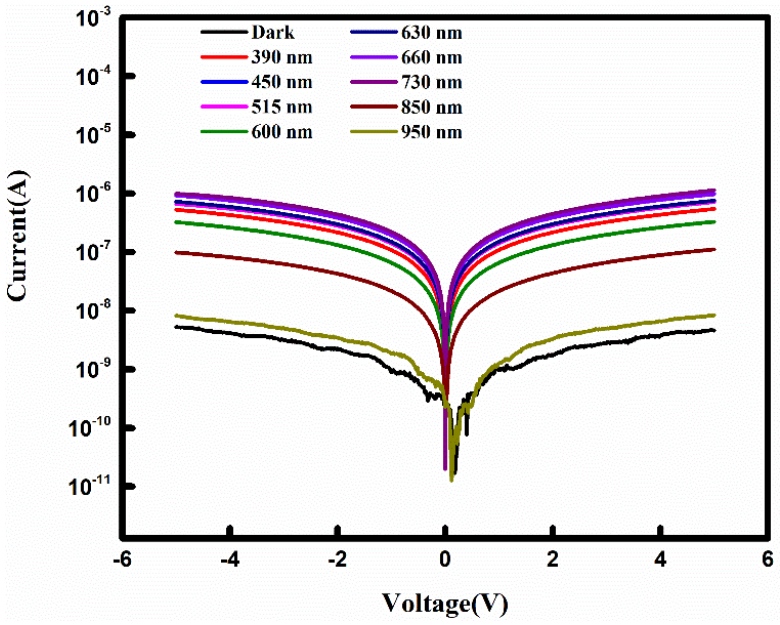

Figure 3- 7: Logarithmic scale IV curves of $MAPbI_3$+PVP+PMMA photoconductor under dark and various monochromatic lights.

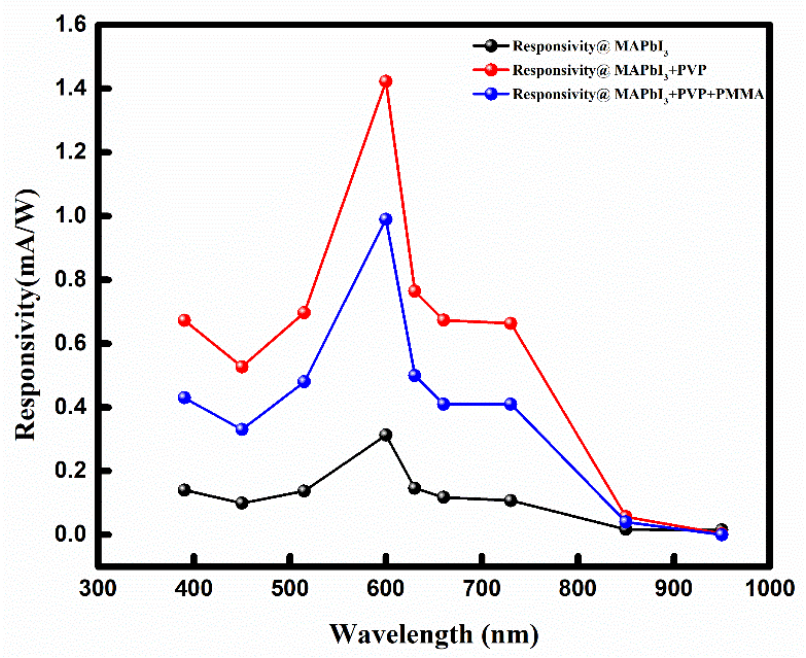

Figure 3- 8: The curve for Responsivity at various wavelengths ranging from 390 nm to 950 nm at a fixed bias of 4V.

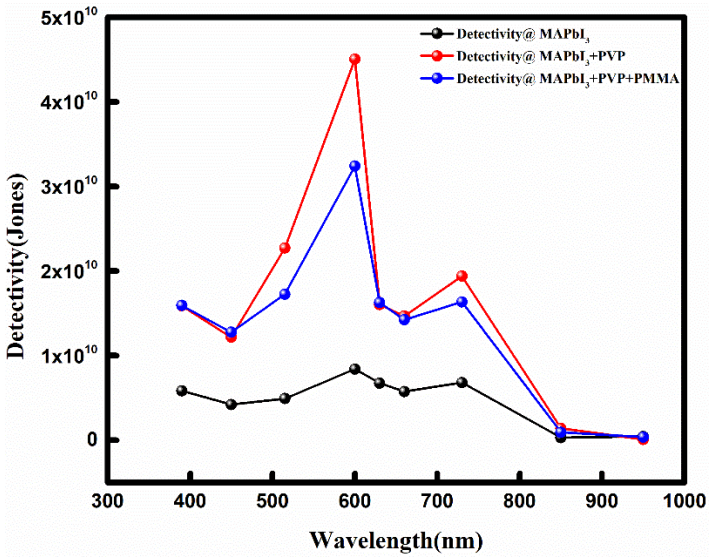

Figure 3- 9: The curve for Detectivity at various wavelengths ranging from 390 nm to 950 nm at a fixed bias of 4V.

As expected, a significant increase in values of responsivity and detectivity can be seen from the plots above. The shape of the curve is still the same, which means that the device is again highly responsive near 550nm wavelength. Also, we can see nearly zero responsivity and detectivity at 850nm and 950nm, which is due to the band-edge of $MAPbI_3$. The PVP and PMMA treatment significantly

improved the responsivity of the pristine $MAPbI_3$ device, as can be seen in Figure 3-10.

Further, to compare PMMA-treated devices with pristine $MAPbI_3$, we characterized its IV at various intensities under 515nm monochromatic light illumination, which can be seen below in Figure 3-11. Under the illumination of monochromatic 515nm light, this device exhibits a light-to-dark ratio of 1597.54 Which is 1.2 times higher than that of a pristine $MAPbI_3$ photoconductor.

Further normalized Current versus time was plotted (Figure 3-12) to calculate rise and fall time. A lower response time indicates a faster response to incident photons so we can see from the plot that PMMA passivation not only improved the photocurrent and response parameters of pristine $MAPbI_3$ photoconductor but also reduced rise and fall time from 3.152 Sec to 0.227 Sec which is 13.89 times lesser than pristine $MAPbI_3$ photoconductor and 0.217 Sec to 0.192 Sec which is 1.13 time lesser than that of pristine $MAPbI_3$ respectively.

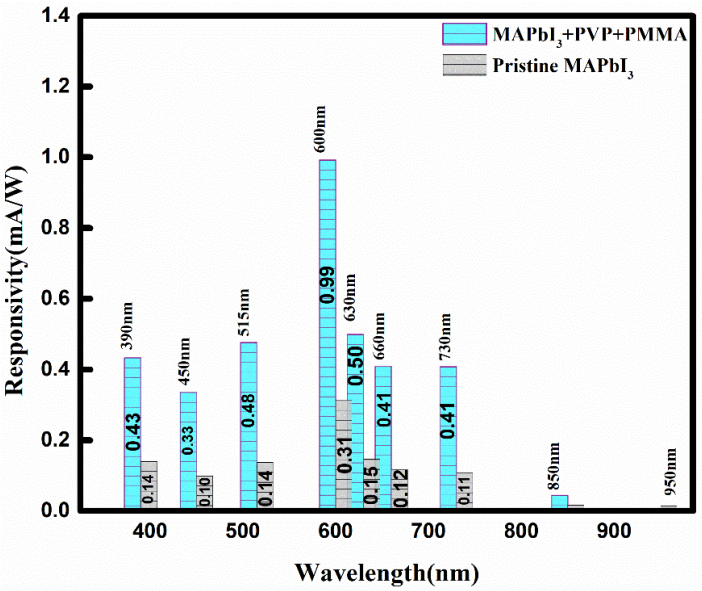

Figure 3- 10: Comparison of responsivity at various wavelengths ranging from 390 nm to 950 nm at a fixed bias of 4V.

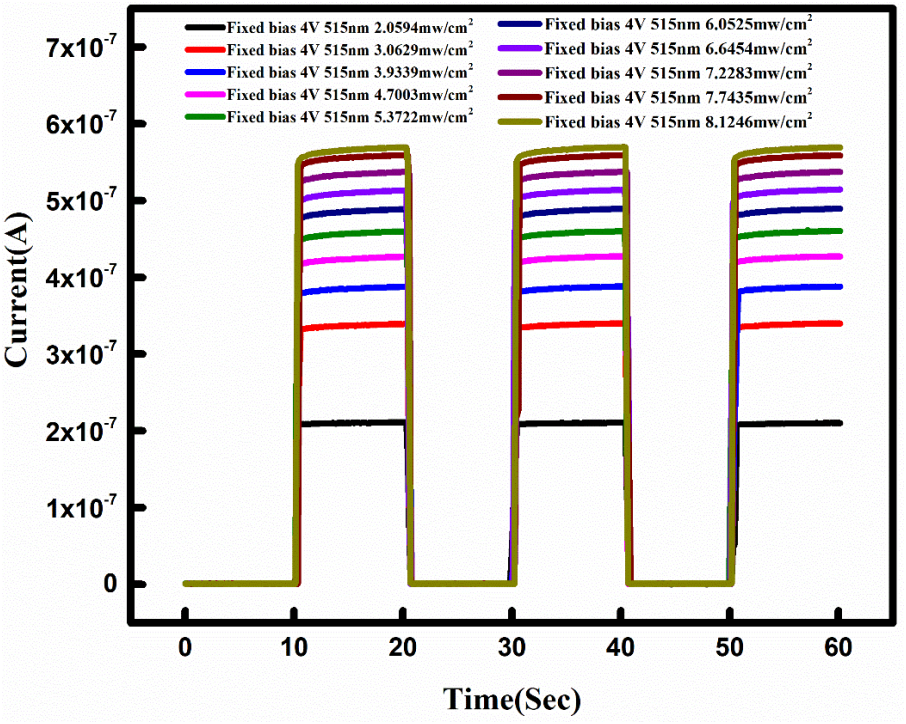

Figure 3- 11: Light-Dark current curves of $MAPbI_3$+PVP+PMMA under 515nm monochromatic light illumination at a fixed bias of 4V.

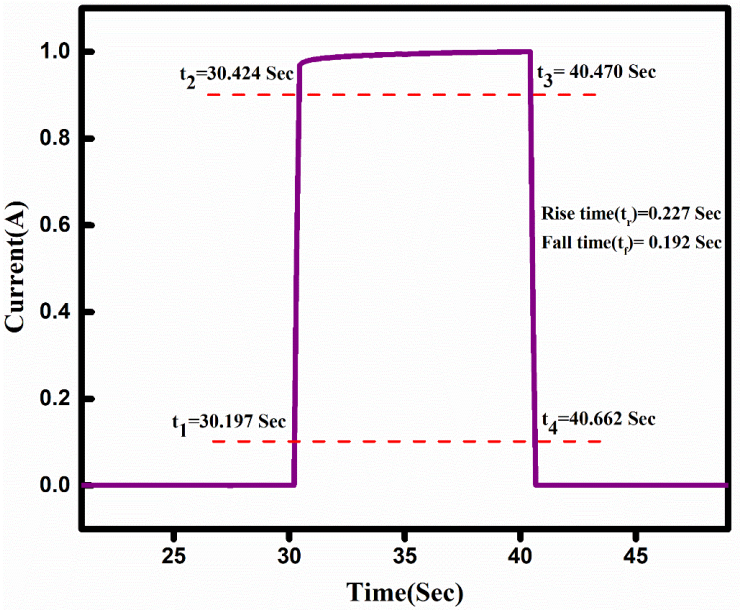

Figure 3- 12: The normalized photocurrent over a varied duration of time at incident light of 515nm with an 8.1246 mW/cm^2 intensity for calculation of rise and fall time of $MAPbI_3$+PVP+PMMA devices.

A lower response time indicates a faster response to incident photons so we can see from the plot that PMMA passivation not only improved the photocurrent and response parameters of pristine $MAPbI_3$ photoconductor but also reduced rise and fall time from 3.152 Sec to 0.227 Sec which is 13.89 times lesser than pristine $MAPbI_3$ photoconductor and 0.217 Sec to 0.192 Sec which is 1.13 time lesser than that of pristine $MAPbI_3$ respectively Also, there might be some decrement in various response parameters or photocurrent after PMMA treatment on PVP passivated devices but PMMA treated devices shown 2.06 lower rise time and 0.76 time higher fall time in comparison to only PVP passivated devices.

Further, the curves show the responsivity and detectivity of the device at various wavelengths Figure 3-13 and Figure 3-14. The device showed 0.657 mA/W responsivity and 2.227×10^8jones detectivity at 3.93mW/cm^2 intensity of incident 515nm light.

As expected a significant change in values of responsivity and detectivity can be seen. So further, to get a proper idea about the change in values of responsivity at each intensity value before and after polymer treatment, figures 3-15 can be referred to.

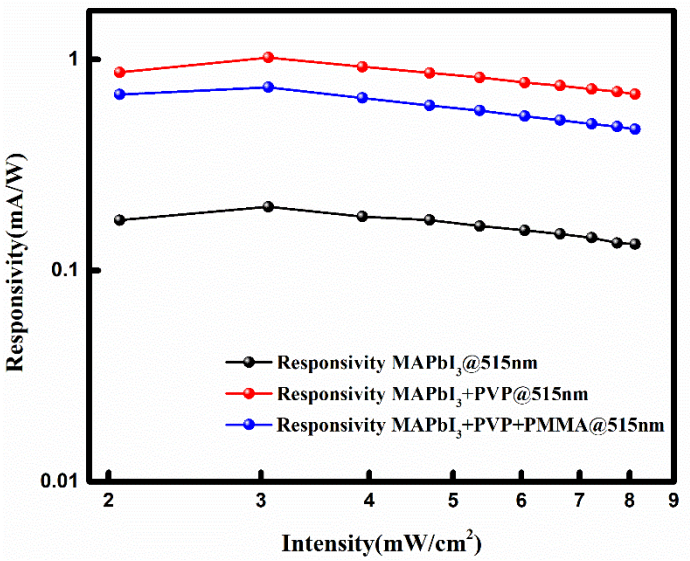

Figure 3- 13: The plot for Responsivity variation with optical power density under 515nm monochromatic light illumination.

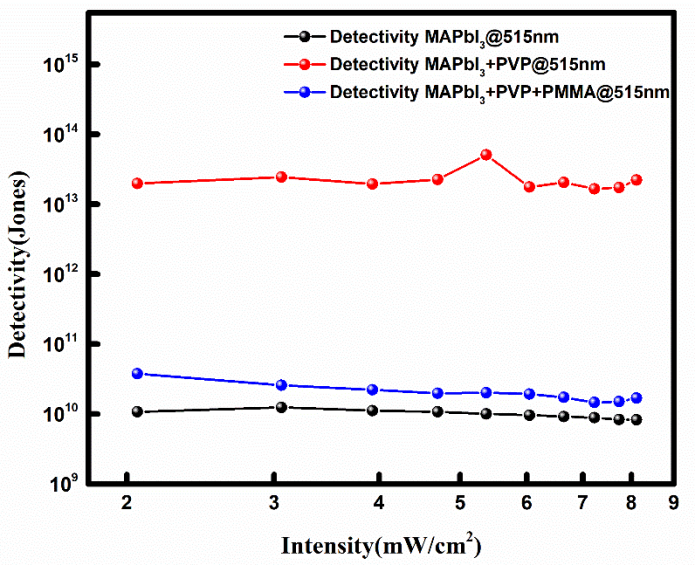

Figure 3- 14: The plot for Detectivity variation with optical power density under 515nm monochromatic light illumination.

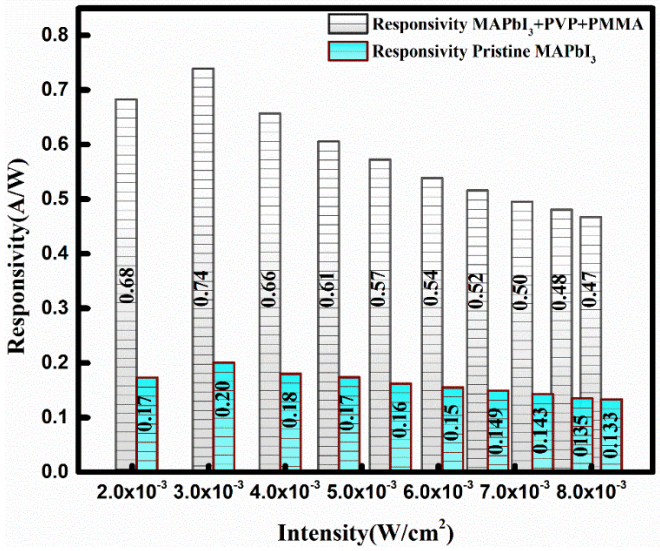

Figure 3- 15: Comparison of responsivity at various intensities under 515nm monochromatic light illumination at a fixed bias of 4V.

As higher LDR ensures precision and accuracy in converting incident light to electrical signals along with a high signal-to-noise ratio allowing accurate detection of weak signals it can be seen from figure 3-16 that this $MAPbI_3$+PVP+PMMA photoconductor exhibited LDR of 151dB whereas pristine $MAPbI_3$ could exhibit LDR of 125dB only.

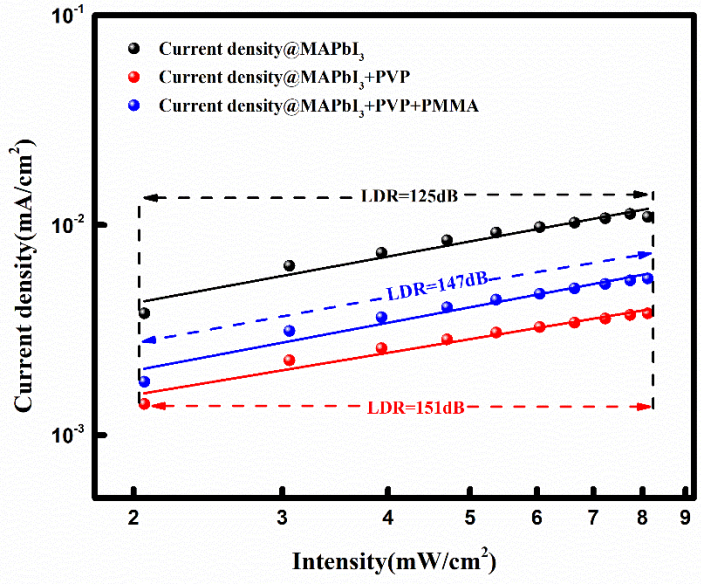

Figure 3- 16: The plot for Current versus Intensity for $MAPbI_3$+PVP+PMMA under 515nm monochromatic light illumination at Fixed 4V bias for calculation of LDR.

Further, we calculated EQE for PMMA-treated devices to have an idea about EQE enhancement for these devices than pristine ones. So, figure 3-17 shows the variation of EQE with increment in wavelength.

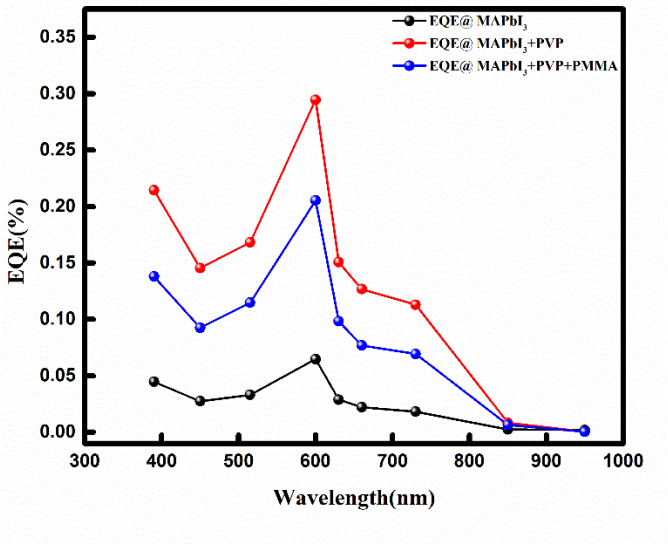

Figure 3- 17: The plot for Wavelength versus EQE for $MAPbI_3$+PVP+PMMA and pristine $MAPbI_3$.

As we can see that PVP and PMMA treatment of pristine $MAPbI_3$ devices increased EQE so much it indicates that a greater number of incident photons are

now absorbed to generate a greater number of charges and hence it increases the electrical conductivity of this device than pristine one which results in photocurrent as well as overall response parameters of this photoconductor.

Further, to get a comparison with an increase in EQE with an increment in intensity at a particular wavelength of 515nm, figure 3-18 can be referred to.

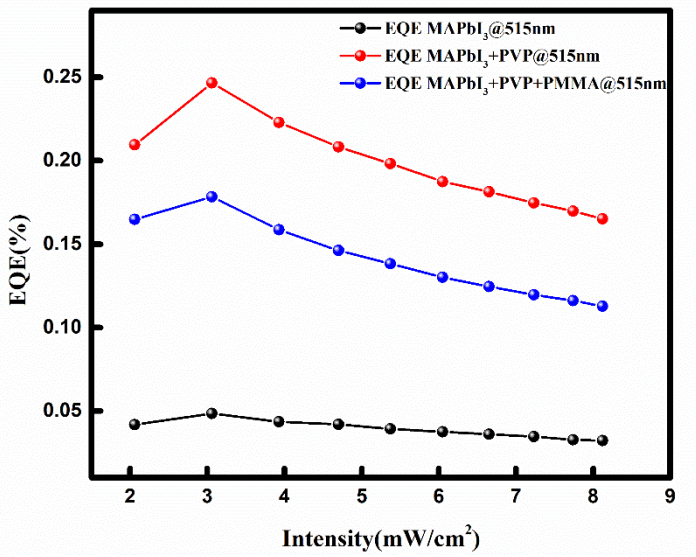

Figure 3- 18: The plot for EQE versus Intensity for $MAPbI_3$+PVP+PMMA and pristine $MAPbI_3$ device using 515nm wavelength light at fixed 4V bias.

The curve follows the same trend, but with an enhancement in EQE , so it also enhanced the performance of the pristine $MAPbI_3$ device at a particular wavelength of 515nm.

Further, as we discussed above, stability was an issue for pristine $MAPbI_3$ as well as PVP-treated $MAPbI_3$, and both devices could only last for 4 days. So, to compare the stability of PMMA-treated devices and these devices, Figure 3-19 can be referred to.

As can be seen from the curve, pristine and PVP-treated $MAPbI_3$ started degrading in just four days, and their degradation rate is too fast. Along with this, they showed 3 orders of magnitude change in just 5-6 days. But in the case of PMMA treated $MAPbI_3$, the rate of degradation was seen to be very low. Also, in 11 days, this device showed just one magnitude order change in photocurrent

value, whereas PVP-treated $MAPbI_3$ and pristine $MAPbI_3$ showed one order magnitude change in just 4 days, which can be seen in Figure 3-19 below. So PMMA treatment enhanced the stability of $MAPbI_3$ photoconductor, and this resulted in enhancement of photocurrent as well as various response parameters discussed above.

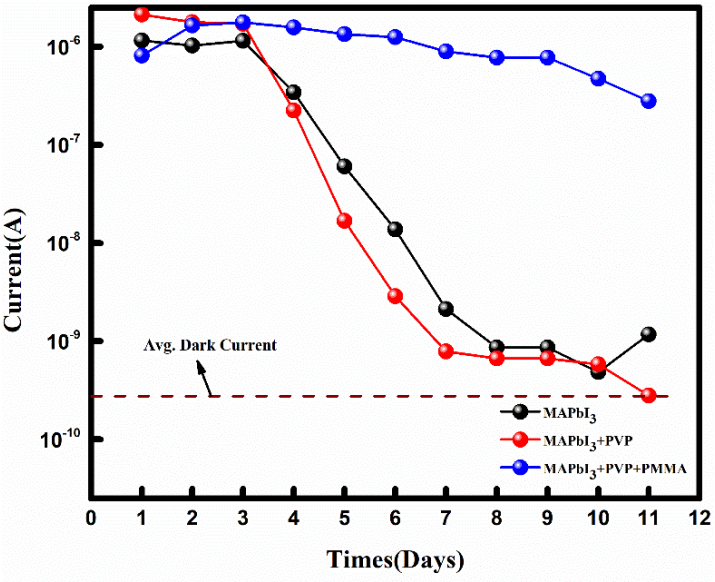

Figure 3- 19: Number of days versus photocurrent exhibited by polymer passivated (PMMA) and pristine $MAPbI_3$ photoconductor.

From Figure 3-20, it can be seen that PVP and PMMA-treated devices showed approximately 34% of the photocurrent on the first day even after 11 days, whereas both the pristine-$MAPbI_3$ and PVP-treated $MAPbI_3$ lost full of the photocurrent on the 6^{th} day. As can be seen, a significant change occurred in the photocurrent of these two devices on the 4^{th} day, and further, they continued showing a decrement in photocurrent value, which indicates their significant degradation of $MAPbI_3$ and PVP-treated $MAPbI_3$ on the 4^{th} day. Further, it can be seen from the curve that the rate of decrement is also higher in pristine-$MAPbI_3$ and PVP-treated $MAPbI_3$ devices. So, PMMA treatment enhances the stability of devices, and PMMA-treated devices showed enhancement of response parameters as well as improvement in rise and fall time as compared to pristine-$MAPbI_3$ devices.

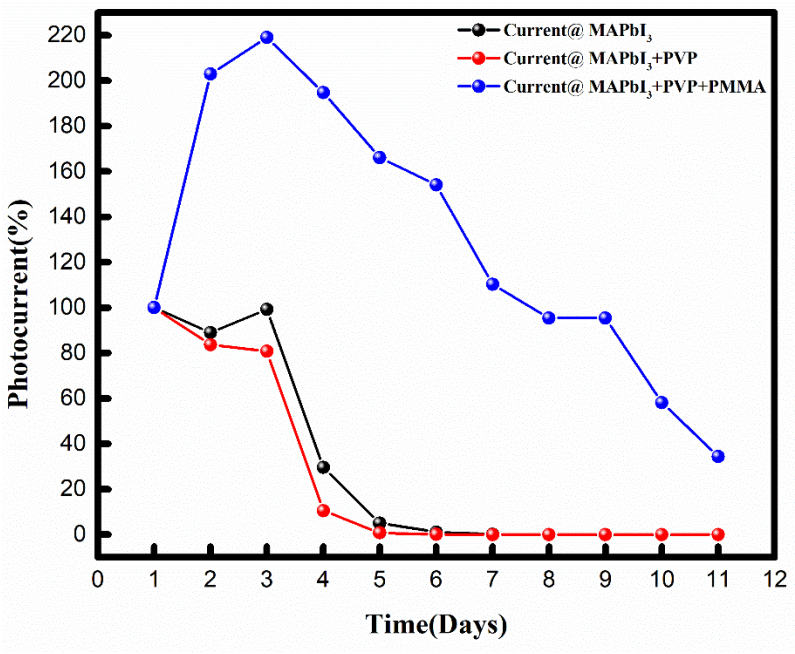

Figure 3- 20: Photocurrent stability analysis of polymer-treated and pristine-$MAPbI_3$ devices over varied duration of time.

Chapter 4: Conclusion

In summary, we have successfully synthesized the $MAPbI_3$ microwire photoconductor and measured its various response parameters. Further, to enhance these various response parameters, we treated it with a polymer PVP, which enhanced its photocurrent 1.44 times more than pristine $MAPbI_3$. PVP treatment enhanced photocurrent and all the response parameters, but it could not enhance its stability. Both the devices started degrading on the fourth day and fell into a dark current on the sixth day. So, to enhance the stability of this device, we treated it by depositing a layer of PMMA on the treated $MAPbI_3$ device, which not only enhanced the photocurrent and response parameters of pristine $MAPbI_3$ but also enhanced its stability than PVP treated as well as pristine $MAPbI_3$. These PMMA-treated devices showed just one order of magnitude fall in photocurrent in ten to eleven days . So, this work opens the way toward improving stability and enhancing various response parameters of $MAPbI_3$ photodetector.

References:

[1] G. Konstantatos and E. H. Sargent, “Nanostructured materials for photon detection,” *Nature Nanotechnology 2010 5:6*, vol. 5, no. 6, pp. 391–400, May 2010, doi: 10.1038/nnano.2010.78.

[2] J. Han, Z. Liang, S. Guo, S. Wang, and S. Qiao, “Photoresponse improvement of a MAPbI3 p-i-n heterojunction photodetector by modifying with a PCBM layer and optimizing ZnO layer thickness,” *Surfaces and Interfaces*, vol. 34, p. 102315, Nov. 2022, doi: 10.1016/J.SURFIN.2022.102315.

[3] L. Gao *et al.*, “Passivated Single-Crystalline CH3NH3PbI3 Nanowire Photodetector with High Detectivity and Polarization Sensitivity,” *Nano Lett*, vol. 16, no. 12, pp. 7446–7454, Dec. 2016, doi: 10.1021/acs.nanolett.6b03119.

[4] G. Li, Y. Wang, L. Huang, and W. Sun, “Research Progress of High-Sensitivity Perovskite Photodetectors: A Review of Photodetectors: Noise, Structure, and Materials,” *ACS Appl Electron Mater*, vol. 4, no. 4, pp. 1485–1505, Apr. 2022, doi: 10.1021/ACSAELM.1C01349/ASSET/IMAGES/LARGE/EL1C01349_0009.JPEG.

[5] W. L. Tsai, C. Y. Chen, Y. T. Wen, L. Yang, Y. L. Cheng, and H. W. Lin, “Band Tunable Microcavity Perovskite Artificial Human Photoreceptors,” *Advanced Materials*, vol. 31, no. 24, p. 1900231, Jun. 2019, doi: 10.1002/ADMA.201900231.

[6] Y. Fu, H. Zhu, J. Chen, M. P. Hautzinger, X. Y. Zhu, and S. Jin, “Metal halide perovskite nanostructures for optoelectronic applications and the study of physical properties,” *Nature Reviews Materials 2019 4:3*, vol. 4, no. 3, pp. 169–188, Feb. 2019, doi: 10.1038/s41578-019-0080-9.

[7] X. Hu *et al.*, “High-performance flexible broadband photodetector based on organolead halide perovskite,” *Adv Funct Mater*, vol. 24, no. 46, pp. 7373–7380, Dec. 2014, doi: 10.1002/adfm.201402020.

[8] W. Tian, C. Zhao, J. Leng, R. Cui, and S. Jin, “Visualizing Carrier Diffusion in Individual Single-Crystal Organolead Halide Perovskite Nanowires and Nanoplates,” *J Am Chem Soc*, vol. 137, no. 39, pp. 12458–12461, Oct. 2015, doi: 10.1021/jacs.5b08045.

[9] A. K. Jena, A. Kulkarni, and T. Miyasaka, “Halide Perovskite Photovoltaics: Background, Status, and Future Prospects,” *Chem Rev*, vol. 119, no. 5, pp. 3036–3103, Mar. 2019, doi: 10.1021/ACS.CHEMREV.8B00539.

[10] Y. Li, Z. Li, F. Liu, and J. Wei, “Defects and passivation in perovskite solar cells,” *Surf Innov*, vol. 10, no. 1, pp. 326–343, Dec. 2021, doi: 10.1680/JSUIN.21.00058/ASSET/IMAGES/SMALL/JSUIN10-0003-F8.GIF.

[11] J. A. Christians, P. A. Miranda Herrera, and P. V. Kamat, “Transformation of the excited state and photovoltaic efficiency of CH3NH3PbI3 perovskite upon controlled exposure to humidified air,” *J Am Chem Soc*, vol. 137, no. 4, pp. 1530–1538, Feb. 2015, doi: 10.1021/JA511132A/SUPPL_FILE/JA511132A_SI_002.AVI.

[12] N. Ahn *et al.*, “Trapped charge-driven degradation of perovskite solar cells,” *Nature Communications 2016 7:1*, vol. 7, no. 1, pp. 1–9, Nov. 2016, doi: 10.1038/ncomms13422.

[13] W. Deng *et al.*, “Aligned Single-Crystalline Perovskite Microwire Arrays for High-Performance Flexible Image Sensors with Long-Term Stability,” *Advanced Materials*, vol. 28, no. 11, pp. 2201–2208, Mar. 2016, doi: 10.1002/adma.201505126.

[14] F. Gao, Y. Zhao, X. Zhang, and J. You, “Recent Progresses on Defect Passivation toward Efficient Perovskite Solar Cells,” *Adv Energy Mater*, vol. 10, no. 13, Apr. 2020, doi: 10.1002/AENM.201902650.

[15] Y. Yang *et al.*, “Top and bottom surfaces limit carrier lifetime in lead iodide perovskite films,” *Nature Energy 2017 2:2*, vol. 2, no. 2, pp. 1–7, Jan. 2017, doi: 10.1038/nenergy.2016.207.

[16] Y. Yang *et al.*, “Low surface recombination velocity in solution-grown CH3NH3PbBr3 perovskite single crystal,” *Nat Commun*, vol. 6, Aug. 2015, doi: 10.1038/NCOMMS8961.

[17] J. Yan *et al.*, “Enhanced perovskite crystallization by the polyvinylpyrrolidone additive for high efficiency solar cells,” *Sustain Energy Fuels*, vol. 3, no. 12, pp. 3448–3454, 2019, doi: 10.1039/c9se00632j.